Supporting Information

Quantum Mechanics/Molecular Mechanics Insights into the Enantioselectivity of the *O*-Acetylation of *(R,S)*-Propranolol Catalyzed by *Candida antarctica* Lipase B

Andrés M. Escorcia, Kakali Sen, Martha C. Daza, Markus Doerr, and Walter Thiel**

[*]M.D.: Grupo de Bioquímica Teórica, Universidad Industrial de Santander, Cra 27 Calle 9, Bucaramanga, Colombia. Email: mhodoerr@uis.edu.co

[*]W.T.: Max-Planck-Institut für Kohlenforschung, Kaiser-Wilhelm-Platz 1, 45470 Mülheim, Germany. Email: thiel@kofo.mpg.de

Content:

1. Details about the computational methods

1.1. CHARMM parameters for the acylated serine (SEA)

A new residue was defined during preparation of the acyl-enzyme corresponding to the acylated serine. This residue was labeled SEA. The topology for the SEA residue is shown below. CHARMM force field parameters for SEA were adopted from serine and methyl acetate. Parameters missing for describing the bond OS-CT2 and the angle bending OS-CT2-CT1 were assigned in analogy to the parameters for OSL-CTL2-CTL1 and OSL-CTL2 in lipids (par_all27_prot_lipid.prm).

!!!!!!!!!!!!!!!!!!!!!SEA TOPOLOGY!!!!!!!!!!!!!!!!!!!!!!!!

```
RESI SEA                0.00
GROUP
ATOM   N     NH1   -0.47
ATOM   HN    H      0.31    !          |
ATOM   CA    CT1    0.07    !    HN-N     H21      OE   H11
ATOM   HA    HB     0.09    !          |      |          ||     |
GROUP                       !    HA-CA--C2--OM-CE--C1-H12
ATOM   C1    CT3   -0.17    !          |      |                |
ATOM   CE    CD     0.63    !      O=C     H23             H13
ATOM   OM    OS    -0.34    !          |
ATOM   C2    CT2   -0.05
ATOM   OE    OB    -0.52
ATOM   H11   HA    0.09
ATOM   H12   HA    0.09
ATOM   H13   HA    0.09
ATOM   H21   HA    0.09
ATOM   H23   HA    0.09
GROUP
ATOM   C     C      0.51
ATOM   O     O     -0.51
BOND   C2 CA   OM C2   N HN   N  CA
BOND   C  CA   C +N   CA HA   C2 H21
BOND   C2 H23   OM CE   C1 CE
BOND   C1 H11   C1 H12   C1 H13
DOUBLE   O  C   CE  OE
IMPR   N -C CA HN   C CA +N O   CE C1 OM OE
CMAP   -C  N  CA  C   N  CA  C  +N
```

DONOR HN N
ACCEPTOR OM
ACCEPTOR O C
ACCEPTOR OE CE

1.2. MD setup for MD simulation of AcCalB (docking target)

First, the positions of all hydrogen atoms in the acylenzyme were optimized performing 500 steps of a steepest descent (SD) energy minimization, keeping all other atom coordinates fixed. In this and all subsequent steps all distances involving hydrogen atoms were constrained by SHAKE [1]. Then a sphere of 40 Å radius containing 4454 toluene molecules cut out from an equilibrated simulation of toluene under periodic boundary conditions was superimposed on the enzymatic system, centered at the alpha carbon of the acetylated serine (SEA:CA). All added toluene molecules whose non-hydrogen atoms were within 2.8 Å of any existing non-hydrogen atom were deleted. This solvent sphere covered the entire enzyme. An active region including all residues within 30 Å of the SEA:CA atom was defined. All atoms of protein residues outside this active region were kept fixed during the MD simulations. To preserve the shape of the solvent sphere and to prevent evaporation of solvent molecules in the MD simulations, toluene molecules and crystal waters were restrained by a quartic spherical boundary potential which is zero until 38.5 Å, has a shallow minimum of -0.25 kcal mol^{-1} at 39.5 Å and increases at larger distances. This was done using the parameters FORCE = 0.2, P1 = 2.25, and DROFF = 38.5. Thereafter the toluene molecules within the sphere and the crystal waters were geometry-optimized, performing first 250 steps of steepest descent (SD) followed by 250 steps of adapted-basis Newton–Raphson (ABNR) minimization, keeping all other atoms fixed. We performed two more minimizations of 250 steps each (SD and ABNR), optimizing the active region with the water and toluene molecules, adding harmonic position restraints with a force constant k = 30 mol $Å^{-2}$ on the active region. Then a heating molecular dynamics simulation (15000 steps) was performed starting at 50 K and ending at 300 K, raising the temperature in steps of 10 K every 100 MD steps. The Verlet algorithm was used with a time step of 1 fs. This solvation procedure was repeated 12 times, and in the last two cycles the number of steps used in the dynamics was increased to 30000. Resolvation is necessary since volume contraction of the solvent results from the enhanced interaction and relaxation of toluene on the enzyme surface. During the solvation procedure, harmonic positional restraints were applied to the protein atoms in the active region, which were successively lowered in each of the iterations. Finally, all constraints were removed and a production molecular dynamics simulation of 2 ns was run to complete the preparation of the acylenzyme. Again, the temperature was raised from 50 K to 300 K in steps of 10 K every 100 MD steps. The first 10 ps of the MD simulations were regarded as an equilibration phase and the following 1990 ps were analyzed.

Nonbonded interactions in all CHARMM simulations were treated using group-based extended electrostatics [2]. In this approach, the electrostatic interactions between particles closer than a cutoff distance (14 Å in our case) are treated by the conventional pairwise additive scheme, while the interactions at larger distance are approximated by a computationally cheaper multipole approach.

Active region: All the residues of the protein were active, only 80 atoms corresponding to some of the surface residues of the protein were fixed, crystal waters and all toluene molecules were also active.

1.3. Docking procedure for building TI-2

The protein was treated as a rigid receptor and five water molecules (HOH130, HOH149, HOH238, HOH265, HOH285) were removed from the active site to accommodate the substrate. The TI-2 structures were built varying the dihedral angles shown in Figure S1, starting from the torsion angles of *R*- and *S*-propranolol in the corresponding AcCalB-propranolol Michaelis complexes [3]. Moreover, we ensured that steric contacts with the residues of the CalB binding pocket were avoided and all essential hydrogen bonds for the catalytic process were formed.

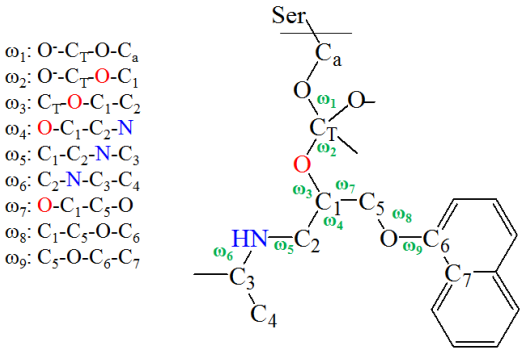

Figure S1. Torsion angles (ω_1-ω_9) considered for building TI-2.

1.4. Post-docking optimization of TI-2

Three consecutive energy minimizations were performed: (1) a fixed constraint was applied to the protein backbone and all remaining parts of the systems were harmonically restrained (k = 30 mol Å^{-2}) in 100 steps of a steepest-descent minimization; (2) the protein backbone was kept fixed, the side chains and crystal waters were harmonically restrained and the docked ligand was free to move in 800 steps of a steepest decent minimization followed by 550 steps of an ABNR minimization; (3) only the backbone was kept fixed, with the rest of the system free to move in two minimizations of 2500 steps each (SD and ABNR).

1.5. MD simulations of TI-2

The same MD setup as for AcCalB (see section 1.2) with some modifications in the resolvation procedure was used, treating the docked ligand as part of the active region. Furthermore, different initial velocity distributions were used, corresponding to values of the random seed parameter iseed of 314159 and 835. The MD simulations carried out using the iseed value 835 are indicated by *.

1.6. PES scans along the dihedral angles of *R*-1-methyl-3-(1-naphthoxy)-2-propanol

The structure of the model compound used for the PES scans along the dihedral angles involved in the naphthoxy side chain of propranolol is shown in Figure S2. Relaxed PES scans were performed at the B3LYP/TZVP level along the torsion angles ω_7-ω_9.

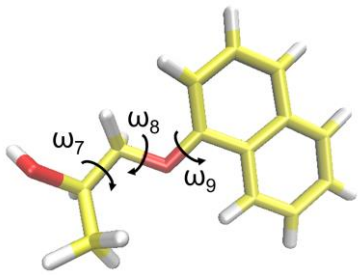

Figure S2. *R*-1-methyl-3-(1-naphthoxy)-2-propanol.

2. Docking results

The TI-2 structures generated from the docking procedure were named TI-R or TI-S to emphasize whether it is the *R* or *S* enantiomer, followed by 1, 2, 3, … according to the order in which they were created. A total of 6 structures were identified for *R*- and *S*-propranolol, four in binding mode I (TI-R1(S1) – TI-R4(S4)) and two in binding mode II (TI-R5(S5) – TI-R6(S6)) (see Figures S3-S4). After post-docking optimization, superimposition of the protein structure of TI-2 and the CalB crystal structure showed only minor displacements with RMSD values of about 0.55 Å (see Table S1). Furthermore, all optimized TI-2 structures contain the essential hydrogen bonds for the catalytic process (see Table S2), so they are possible productive binding modes of the substrate. The main differences between the TI-2 structures concern the presence of an additional hydrogen bond in the case of *R*-propranolol in binding mode I (between its amino group and the carbonyl oxygen of Thr40; Sub:*H*-Thr40:O), which is only formed in one of the TI-2 structures of *S*-propranolol (in binding mode I), and the interactions between the propranolol side chains and the surrounding protein residues. All these interactions are involved in the stabilization of TI-2, so they are partly considered as responsible for the experimentally observed enantioselectivity (see below).

Table S1

RMSD values for all heavy atoms of the protein in the optimized TI-2 structures with respect to the crystal structure of CalB.

R-propranolol		*S*-propranolol	
TI-2	RMSD (Å)	TI-2	RMSD (Å)
TI-R1	0.555	TI-S1	0.554
TI-R2	0.553	TI-S2	0.554
TI-R3	0.554	TI-S3	0.558
TI-R4	0.552	TI-S4	0.553
TI-R5	0.553	TI-S5	0.553
TI-R6	0.554	TI-S6	0.554

2.1. Analysis of the TI-2 structures of *R*- and *S*-propranolol in binding mode I after post-docking optimization

In the TI-2 structures of *R*- and *S*-propranolol in binding mode I, the naphthyl group of propranolol is positioned in the large pocket of CalB in four different orientations, where it is stabilized by the residues Thr138, Leu140, Ala141, Leu144, Ile189 and Ile285 through CH-π interactions. This type of interaction is also present between the isopropylamine side chain of propranolol and the residue Trp104 in the medium pocket of CalB, involving the six-membered ring of this residue, in agreement with its higher propensity to form CH-π interactions compared with the five-member ring [4]. As the strength of a CH-π interaction depends on its distance and directionality (the stronger the interaction, the stronger the trend to linearity) [5], the stabilization of each TI-2 in binding mode I is expected to depend strongly on the orientation of the side chains of propranolol in the binding pocket, especially that of its naphthyl group due to its bulky size and its π-donor character. Therefore these CH-π interactions are

expected to play an important role in the stabilization of the corresponding transition states (TSs) and thus in the enantioselectivity of the reaction. The isopropylamine side chain is also stabilized through hydrophobic interactions with the surrounding aliphatic residues of the medium pocket (namely, Leu278 and Ala281). However, these interactions are similar in all structures and are not expected to have a major influence on the stabilization of TI-2 in comparison to the CH-π interactions.

The distances for the CH-π interactions present in the TI-2 structures in binding mode I are shown in Figure S5. Comparison of the CH-π interactions in the TI-2 structures of *R*-propranolol and *S*-propranolol shows (see the orientation of the naphthyl group) that there are major differences for TI-R1 and TI-R2 relative to TI-S1 and TI-S2, respectively. In TI-R1 and TI-S1 the naphthyl group of propranolol is pointing toward the entrance of the binding pocket, where is strongly stabilized through CH-π interactions with the residues Ile189 and Val154. The side chains of these residues (mainly that of Ile189) are partly directed to the center of the naphthyl rings, allowing for more linear CH-π interactions in comparison to the other residues at the large pocket. Ile189 stabilizes both naphthyl rings while Val154 interacts mainly with the naphthyl ring A (the one which is forming the ether bond in the propranolol molecule). Furthermore, the CH-π interactions with Ile189 are in general stronger in TI-R1 than in TI-S1, while the CH-π interactions with Val154 are stronger in TI-S1. The strongest CH-π interaction with Ile189 in TI-R1 is between the Cγ2 atom of this residue and the center of mass of the naphthyl ring A, with a distance of 3.77 Å, while in TI-S1 the strongest CH-π interaction with Val154 has a distance of 4.35 Å. On the other hand, the CH-π interactions between the isopropyl group of propranolol and Trp104 are slightly stronger in TI-R1. All this plus the additional Sub:*H*-Thr40:O hydrogen bond formed in TI-R1 (see Table S2) suggest a better stabilization of the corresponding TSs involved in the transformation of TI-R1 with respect to those of TI-S1, which would favor the faster transformation of the former.

In TI-R2 and TI-S2, the naphthyl group of propranolol is pointing toward the residues Ile285, Val154 and Leu144. The position of the naphthyl rings in these TI-2 structures allows strong CH-π interactions (trend to linearity) with the residues Ala141, Leu144 and Val154. The CH-π interactions between the naphthyl rings and Val154 (through its Cγ1 and Cγ2 atoms) are stronger in TI-S2 than in TI-R2, while the CH-π interactions with Leu144 (through its Cδ1 atom) are stronger in the latter. In contrast, the CH-π interactions with Ala141 are similar in both structures. On the other hand, the CH-π interactions between the isopropyl group of propranolol and Trp104 are stronger in TI-R2 than in TI-S2. All this suggests a better stabilization of the TSs involved in the transformation of TI-R2 with respect to those of TI-S2, which would lead to a faster transformation of TI-R2 over TI-S2. The Sub:*H*-Thr40:O hydrogen bond is formed in both TI-R2 and TI-S2, therefore it is not considered to have a specific effect on the transformation of TI-R2 relative to TI-S2.

In the other TI-2 structures in binding mode I the CH-π interactions between the naphthyl group of propranolol and the surrounding protein residues are similar for both enantiomers. However, the formation of the Sub:*H*-Thr40:O hydrogen bond in TI-R3 and TI-R4 may contribute to a better stabilization of the corresponding TSs involved in the

TI-2 transformations, such that they are favored over those of TI-S3 and TI-S4, in which this hydrogen bond is not formed.

2.2. Analysis of the TI-2 structures of *R*- and *S*-propranolol in binding mode II after post-docking optimization

In the TI-2 structures of both propranolol enantiomers in binding mode II the naphthyl group of propranolol is positioned in the medium pocket of CalB in two distinct orientations (pointing outward or inward the binding pocket), and it is also stabilized by CH-π interactions with the nonpolar residues Trp104, Ile189, Leu278, Ala281, Ala282 and Ile285. In contrast to binding mode I, in binding mode II the isopropylamine side chain of propranolol is not forming CH-π interactions and is only stabilized by hydrophobic interactions with the surrounding aliphatic residues of the large pocket. These interactions are similar in all TI-2 in binding mode II. Thus, as in binding mode I, the stabilization of the TI-2 structures in binding mode II is expected to depend mainly on the CH-π interactions established between propranolol and the surrounding protein residues. The distances for these CH-π interactions are shown in Figure S6.

Following the same scheme of analysis as for the TI-2 structures in binding mode I, the transformation of TI-R5 is expected to be favored over TI-S5. In these TI-2 structures the naphthyl group of propranolol is pointing toward the entrance of the binding pocket, but it is more exposed toward the entrance of the pocket in TI-S5 than in TI-R5. This affects the strength of the CH-π interactions established with the residues Leu278, Ala281, Ile189 and Trp104. The CH-π interaction between naphthyl ring A and Trp104 is stronger in TI-R5 than in TI-S5. Furthermore, in TI-R5 both naphthyl rings of propranolol are strongly stabilized by Leu278 and Ala281, while in TI-S5 the CH-π interactions between these residues and the naphthyl ring B are partly lost. In addition, considering the orientation of the naphthyl rings in these TI-2 structures, the CH-π interactions with Ala281 and Ile189 (through its Cγ2 atom) are stronger (more linear) in TI-R5 than in TI-S5 (see Figures S3-S4). All this suggests a better stabilization of the TSs involved in the transformation of TI-R5 with respect to those of TI-S5, which would favor a faster transformation of TI-R5.

In TI-R6 and TI-S6 the naphthyl group of propranolol is oriented toward the interior of the binding pocket. This leads to the formation of CH-π interactions between the naphthyl ring B and the residues Ala281 and Leu278 which are stronger than those with naphthyl ring A (judging from the linearity of the interactions). In addition, the residue Trp104 forms a CH-π interaction with this ring. In contrast, the residue Ile189 is interacting mainly with naphthyl ring A. The observed distances for these interactions show that TI-R6 is better stabilized than TI-S6, suggesting a better stabilization of the TSs involved in the transformation of the former.

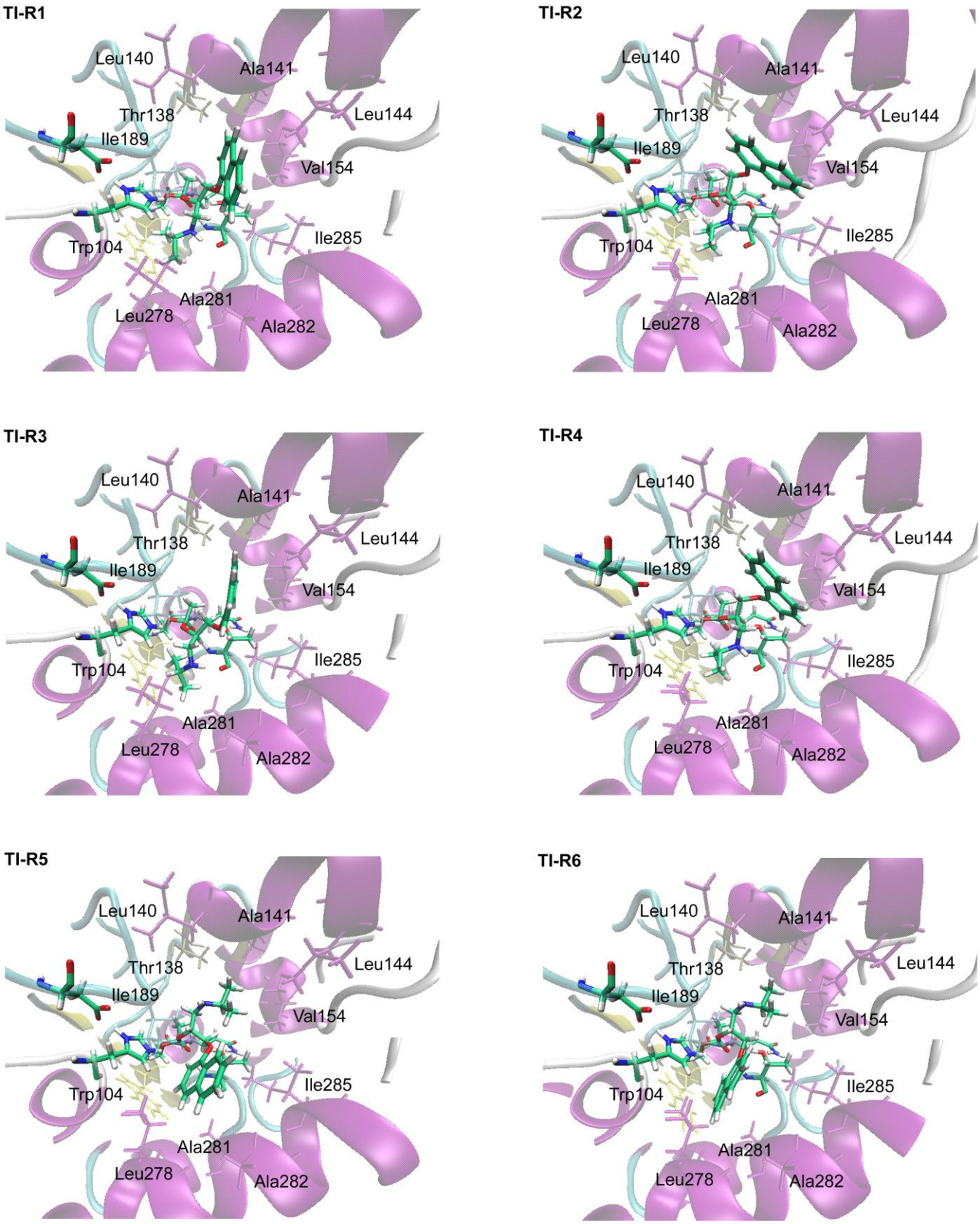

Figure S3. TI-2 structures of *R*-propranolol after post-docking optimization. The TI-2 and the catalytic triad are shown in licorice with the carbon atoms in green. The residues stabilizing the side chains of propranolol in the binding pocket are also shown in licorice, with a unique color indicating the secondary structure to which they belong: α-helix (purple), β-conformation (yellow) and loops (cyan).

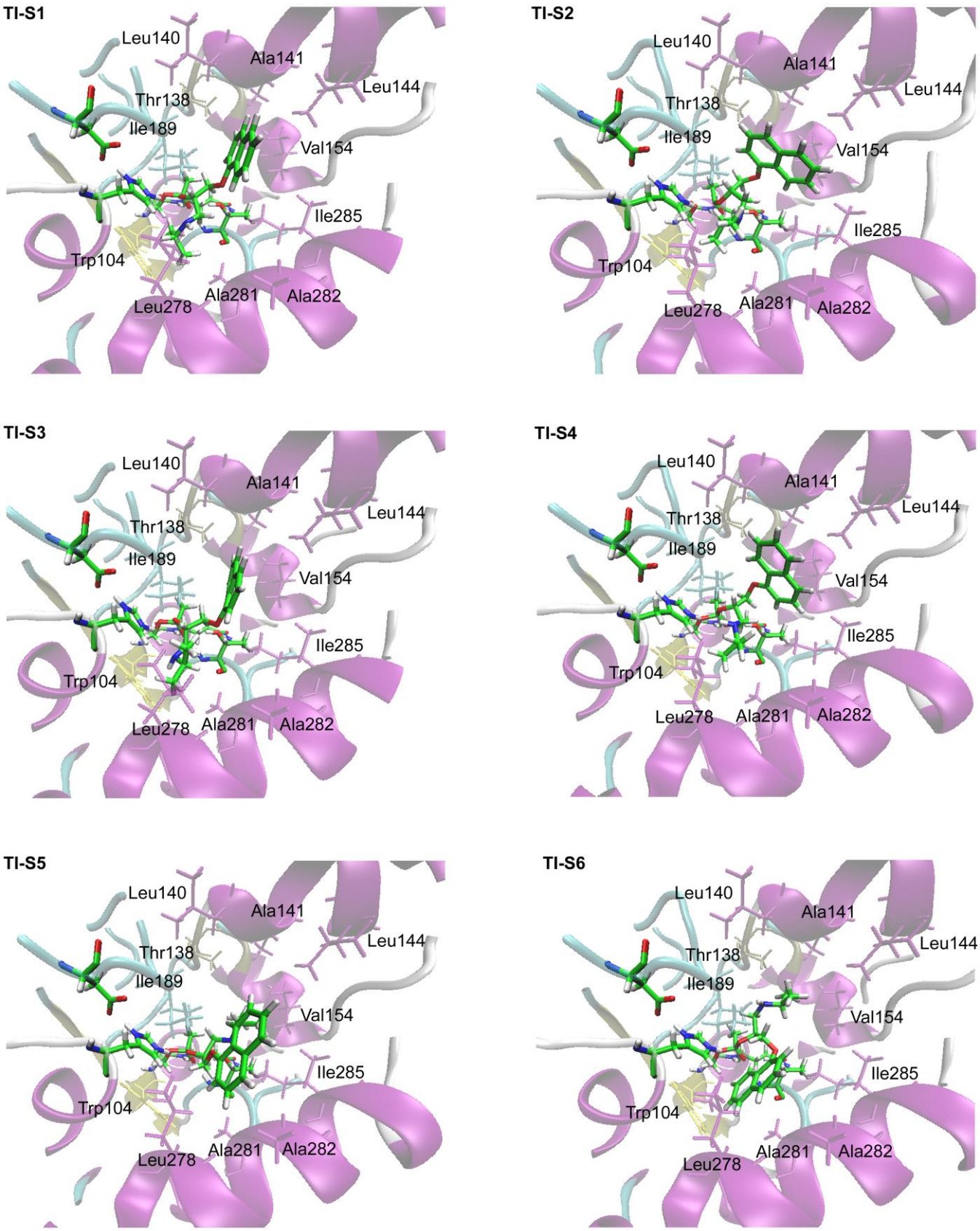

Figure S4. TI-2 structures of *S*-propranolol after post-docking optimization. The TI-2 and the catalytic triad are shown in licorice with the carbon atoms in green. The residues stabilizing the side chains of propranolol in the binding pocket are also shown in licorice, with a unique color indicating the secondary structure to which they belong: α-helix (purple), β-conformation (yellow) and loops (cyan).

Table S2

Hydrogen bond distances and angles of the TI-2 structures of *R*- and *S*-propranolol after optimization[a].

TI-2	SEA:O-Gln106:NH	SEA:O-Thr40:NH	SEA:O-Thr40:OH	His224:**H**-SEA:O_γ	His224:**H**-Sub:**O**	Asp187:O_D-His224:H_{ND}	Sub:*H*-Thr40:O
TI-R1	1.81 (164)	1.70 (165)	2.01 (174)	2.19 (125)	1.74 (159)	1.60 (177)	1.85 (149)
TI-R2	1.78 (161)	1.81 (164)	2.11 (174)	2.06 (124)	1.88 (150)	1.64 (174)	2.39 (106)
TI-R3	1.84 (166)	1.64 (165)	2.01 (172)	2.03 (135)	1.84 (143)	1.62 (166)	1.92 (170)
TI-R4	1.81 (162)	1.77 (165)	2.09 (173)	2.12 (124)	1.87 (150)	1.63 (173)	2.02 (128)
TI-R5	1.92 (155)	1.96 (168)	2.07 (174)	2.02 (124)	1.95 (134)	1.67 (171)	7.70
TI-R6	1.89 (150)	2.18 (169)	2.36 (171)	2.17 (116)	2.09 (123)	1.71 (169)	7.76
TI-S1	1.89 (164)	1.66 (166)	1.95 (173)	2.09 (135)	1.80 (144)	1.60 (168)	3.94
TI-S2	1.72 (160)	1.74 (158)	1.89 (175)	1.83 (139)	2.22 (139)	1.65 (171)	2.52 (113)
TI-S3	2.02 (162)	1.76 (173)	2.12 (170)	2.14 (133)	1.98 (128)	1.64 (164)	4.00
TI-S4	1.93 (158)	1.80 (165)	1.91 (175)	1.92 (132)	1.96 (137)	1.65 (171)	4.72
TI-S5	1.80 (166)	1.67 (164)	2.02 (171)	2.03 (129)	1.79 (149)	1.63 (172)	3.98
TI-S6	1.83 (156)	1.90 (164)	1.99 (172)	2.13 (120)	1.97 (144)	1.67 (173)	7.78

[a] Distances are given in Å. A maximum distance of 3 Å was chosen as a limit to be considered a hydrogen bond. Angles are given in degrees (º) in parentheses. See Figure 4 of the main text for conventions on the atom labels.

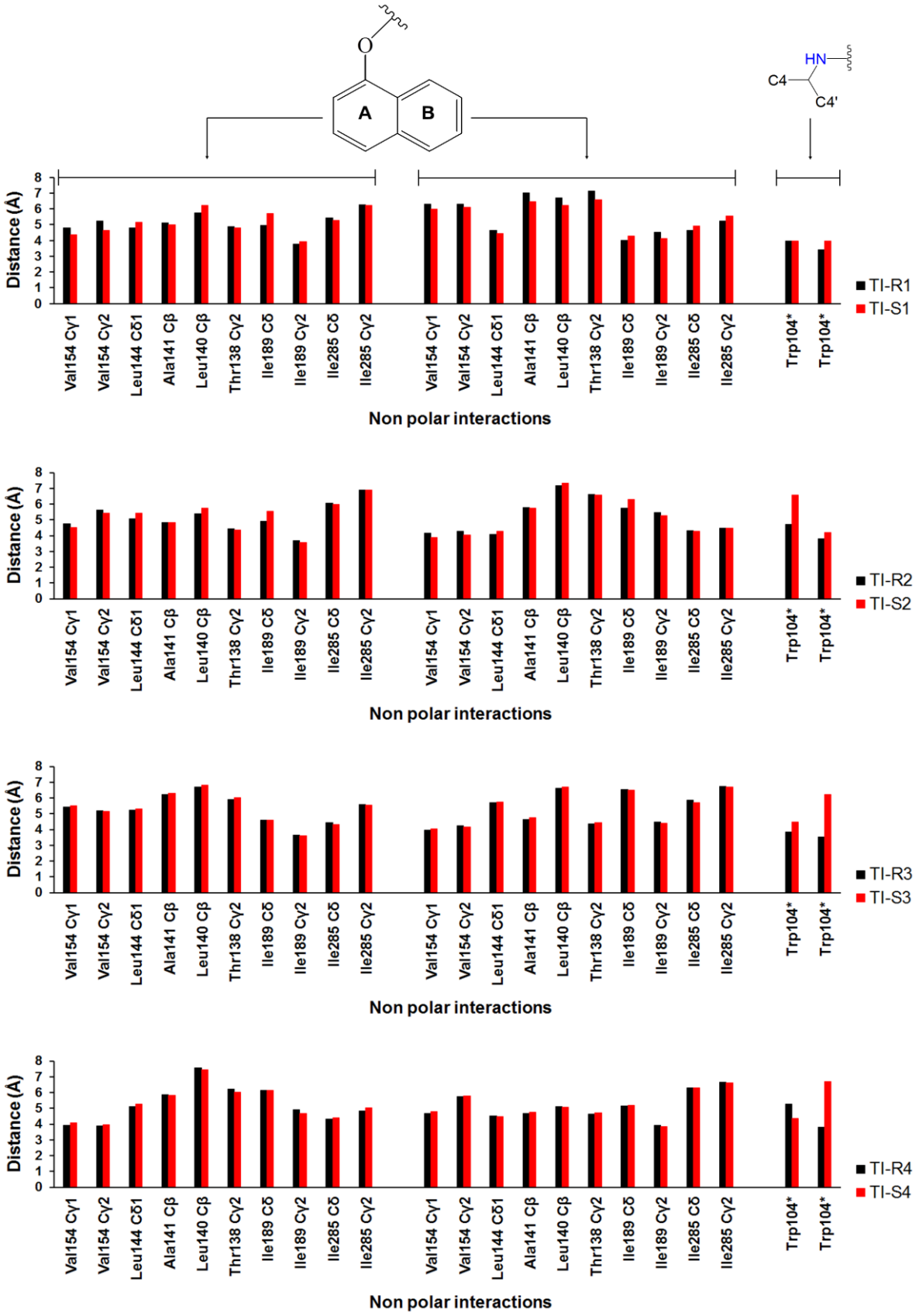

Figure S5. Distances between the side chains (center of mass of the naphthyl rings and of the carbon atoms of the isopropyl methyl groups) of *R*- and *S*-propranolol and the surrounding residues of the binding pocket, in the TI-2 structures in binding mode I after post-docking optimization. Every set of analogous structures (related to the orientation of the naphthyl group) is shown separately. * Center of mass of the six-membered ring.

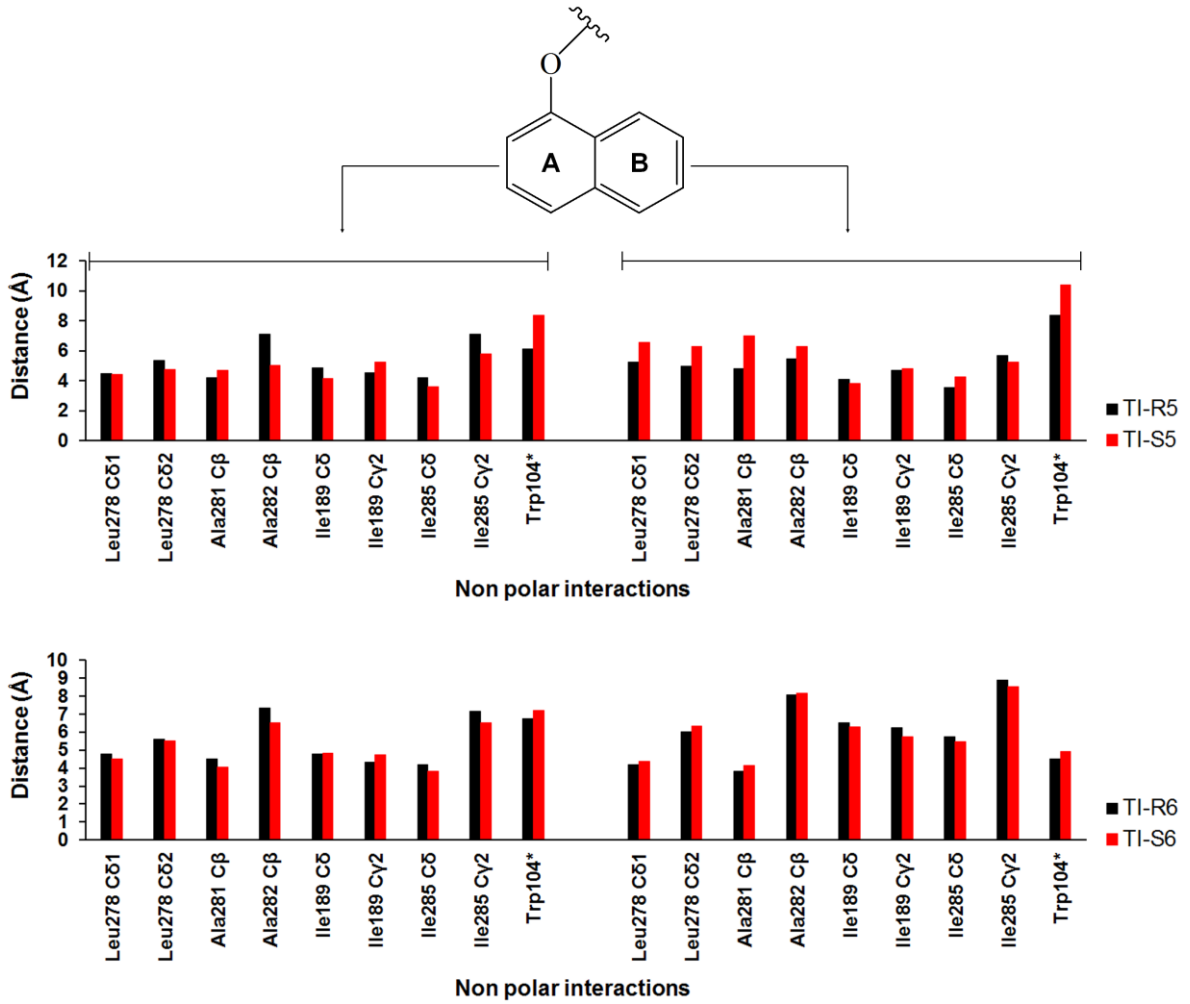

Figure S6. Distances between the centers of mass of naphthyl rings of *R*- and *S*-propranolol and the surrounding residues of the binding pocket, in the TI-2 structures in binding mode II after post-docking optimization. Every set of analogous structures (related to the orientation of the naphthyl group) is shown separately. * Center of mass of the six-membered ring.

3. MD results

CalB does not undergo significant conformational changes during the MD simulations, as shown by the average RMSD values (with respect to the CalB crystal structure) for all heavy atoms of the protein backbone (see Table S3). The largest average RMSD values observed for the TI-2 structures of *R*- and *S*-propranolol are 1.08 ± 0.17 Å and 1.14 ± 0.22 Å, respectively. Regarding the stability of the essential hydrogen bonds for the catalytic process, some differences are observed for *R*- and *S*-propranolol depending on the binding mode. Furthermore, not all TI-2 are stable throughout the MD simulations. A complete description of the dynamic behavior of the TI-2 structures of both propranolol enantiomers is given below.

Table S3

Average RMSD (with respect to the CalB crystal structure) for all heavy atoms of the protein backbone in the MD simulations of TI-2[a].

TI-2	RMSD	RMSD*
TI-R1	0.95 ± 0.21	0.99 ± 0.15
TI-R2	0.98 ± 0.16	1.03 ± 0.20
TI-R3	1.08 ± 0.17	0.83 ± 0.10
TI-R4	1.00 ± 0.14	0.85 ± 0.12
TI-R5	0.90 ± 0.12	1.02 ± 0.20
TI-R6	0.85 ± 0.11	1.02 ± 0.21
TI-S1	1.00 ± 0.21	1.08 ± 0.16
TI-S2	0.88 ± 0.11	1.10 ± 0.17
TI-S3	0.92 ± 0.14	1.14 ± 0.22
TI-S4	1.02 ± 0.17	0.96 ± 0.13
TI-S5	1.01 ± 0.18	1.08 ± 0.23
TI-S6	0.94 ± 0.17	0.91 ± 0.17

[a] RMSD values are given (in Å) for the two MD simulations with different initial velocity distributions as indicated by *.

3.1. Analysis of the MD simulations of the TI-2 structures of *R*-propranolol

3.1.1. Stability of the essential hydrogen bonds for the catalytic process in the MD simulations of the TI-2 structures of R-propranolol

The time evolution of the essential hydrogen bonds for the catalytic process in the MD simulations of *R*-propranolol is shown in Figures S7-S12. It can be seen that the hydrogen bond between Asp187 and His224 is stable throughout the MD simulations. Furthermore, the average distance of this hydrogen bond is similar in all MD simulations (1.71-1.75 Å; see Table S4). The hydrogen bonds between the oxyanion and the residues of the oxyanion hole are also stable throughout the MD simulations. However, the average distance of the hydrogen bond with Gln106 (SEA:O-Gln106:NH) is different depending on the binding mode of *R*-propranolol. As shown in Table S4, this hydrogen bond is shorter in binding mode II (1.70-1.71 Å) than in binding mode I (1.98-2.01 Å). This is correlated with the dynamic behavior of the hydrogen bonds between the protonated His224 and the reactive oxygen atoms. In the MD simulations for *R*-propranolol in binding mode II the alcohol oxygen (Sub:**O**) is displaced toward the oxyanion hole, leading to a stronger hydrogen bond between the oxyanion and Gln106. In turn, the hydrogen bond between the protonated His224 and the Sub:**O** atom (His224:**H**-Sub:**O**) is disrupted; this interaction has an average distance of 2.09-2.30 Å for the TI-2 structures in binding mode I and 3.21-3.49 Å for those in binding mode II (see Table S4 and Figures S7-S12). Meanwhile, the hydrogen bond between the protonated His224 and the SEA:Oγ atom becomes stronger; this hydrogen bond has an average distance of 2.01-2.14 Å for the TI-2 structures in binding mode I and 1.79-1.81 Å for those in binding mode II (see also Table S4 and Figures S7-S12).

The disruption of the His224:**H**-Sub:**O** hydrogen bond and the displacement of the Sub:**O** atom toward the oxyanion hole in the TI-2 structures in binding mode II indicate that it is difficult for *R*-propranolol in this binding mode to reach an orientation which allows the reaction to proceed [6-8].

3.1.2. Dynamic behavior of R-propranolol throughout the MD simulations of TI-2

In the MD simulations of *R*-propranolol in binding mode I two main TI-2 configurations are identified (TI-R[number]**a** and TI-R[number]**b**), which differ in the orientation of the isopropylamine side chain of propranolol in the medium pocket. Configuration **a** is characterized by the formation of a hydrogen bond between the amino group of *R*-propranolol and Thr40 (Sub:*H*-Thr40:O), while in configuration **b** this hydrogen bond is absent. Propranolol is flipping between these two configurations throughout the MD simulations by rotation of the ω_5 dihedral angle (see Figure S1). The Sub:*H*-Thr40:O hydrogen bond is present more than 50 % of the time in all MD simulations, except in the case of TI-R3 with the second initial velocity distribution, in which it is only present during 96 ps (see Figure S13). Particularly, this hydrogen bond is quite stable in the MD simulations of TI-R1, in which it is found in about 80 % of the simulation time and has an average distance of 2.69 Å (see Table S4). Configuration **a** of TI-R1 is thus most persistent in the MD simulations among all TI-2 structures in binding mode I

(see Table S5). Considering only the orientation of the naphthoxy group of propranolol in the large pocket, TI-R1 and TI-R3 are preferred over TI-R2 and TI-R4. The naphthoxy group preserves its initial orientation throughout the MD simulations of TI-R1 and TI-R3, while in the MD simulations of TI-R2 and TI-R4 it adopts the orientation observed in TI-R1 (after less than 80 ps) and TI-R3 (after less than 570 ps), respectively (see Table S5). Interestingly, in the MD simulations of TI-R1 (and of TI-R2 after 80 ps), the residue Leu140 is reoriented establishing a stronger CH-π interaction with the naphthyl group of propranolol (see Figure S14), which remains stable throughout the MD simulations and is therefore not dependent on the observed change on the orientation of the isopropylamine side chain of propranolol during the simulations. This reorientation of Leu140 is expected to contribute to a better stabilization of TI-R1.

The rotation of the ω_5 dihedral angle is also observed in the MD simulations of the TI-2 structures of *R*-propranolol in binding mode II. This results in the temporal formation of an intramolecular hydrogen bond between the amino and naphthoxy groups of propranolol (Sub:*H*-Sub:O) in the MD simulations of TI-R5 (see Figure S15). Thus two configurations are observed, one in which this hydrogen bond is formed (TI-R5a) and one in which it is absent (TI-R5b). However, as shown in Table S5, TI-R5a is present more often (more than 990 ps) than TI-R5b (less than 500 ps). By contrast, in the MD simulations of TI-R6, distinct configurations are not identified. Considering only the orientation of the naphthoxy group of propranolol in the medium pocket, the TI-2 structures identified in the MD simulations of TI-R5 and TI-R6 are stable throughout the MD trajectories. However, it is important to note that they are different from the starting structures (see Figure S14); during heating and equilibration structural rearrangements occur in response to the movement of the Sub:**O** atom toward the oxyanion hole and the interaction of the naphthyl group with the solvent.

Based on the stability of the essential hydrogen bonds for the catalytic process observed in the MD simulations of the TI-2 structures of *R*-propranolol in binding mode I, as well as on the ability of *R*-propranolol to form the Sub:*H*-Thr40:O hydrogen bond in these TI-2 structures, the transformation of *R*-propranolol is expected to be favored in binding mode I. Particularly, its transformation is expected to be faster when its naphthyl group is pointing toward the exterior of the binding pocket and its isopropylamine side chain is oriented such that the Sub:*H*-Thr40:O hydrogen bond is formed (TI-R1a). This assessment is based on the observed temporal stability of TI-R1a in the MD simulations of TI-R1 (about 1200 ps), which exceeds that of the other *R*-propranolol configurations that also contain the Sub:*H*-Thr40:O hydrogen bond (see Table S5) [9].

Table S4

Hydrogen bond distances[a] involving the TI-2 structures of *R*-propranolol[b] averaged over the 1.5 ns MD simulations[c].

TI-2	SEA:O-Gln106:NH	SEA:O-Thr40:NH	SEA:O-Thr40:OH	His224:**H**-SEA:O_γ	His224:**H**-Sub:**O**[d]	Asp187:O_D-His224:H_{ND}	Sub:*H*-Thr40:O
TI-R1	1.99 (0.15)	1.81 (0.14)	1.70 (0.14)	2.14 (0.25)	2.10 (0.31)	1.72 (0.11)	2.69 (0.64)
TI-R1*	1.98 (0.15)	1.82 (0.12)	1.71 (0.12)	2.13 (0.25)	2.14 (0.28)	1.73 (0.11)	2.69 (0.78)
TI-R2	1.99 (0.15)	1.83 (0.15)	1.70 (0.12)	2.05 (0.23)	2.15 (0.28)	1.73 (0.13)	3.30 (1.05)
TI-R2*	1.99 (0.15)	1.81 (0.14)	1.72 (0.13)	2.12 (0.25)	2.09 (0.26)	1.72 (0.11)	3.12 (1.01)
TI-R3	2.01 (0.15)	1.75 (0.11)	1.72 (0.13)	2.03 (0.24)	2.14 (0.33)	1.71 (0.11)	2.81 (0.64)
TI-R3*	1.99 (0.15)	1.75 (0.11)	1.73 (0.13)	2.09 (0.25)	2.09 (0.31)	1.72 (0.11)	5.08 (0.78)
TI-R4	1.99 (0.15)	1.79 (0.15)	1.72 (0.13)	2.04 (0.24)	2.18 (0.37)	1.72 (0.11)	2.73 (0.70)
TI-R4*	1.98 (0.15)	1.81 (0.17)	1.71 (0.13)	2.01 (0.25)	2.30 (0.41)	1.72 (0.11)	3.01 (0.60)
TI-R5	1.70 (0.09)	1.76 (0.12)	1.65 (0.10)	1.80 (0.11)	3.24 (0.31)	1.72 (0.12)	⋯
TI-R5*	1.70 (0.09)	1.78 (0.13)	1.65 (0.10)	1.79 (0.11)	3.23 (0.32)	1.72 (0.12)	⋯
TI-R6	1.71 (0.09)	1.73 (0.10)	1.66 (0.10)	1.79 (0.10)	3.49 (0.22)	1.75 (0.14)	⋯
TI-R6*	1.70 (0.10)	1.79 (0.13)	1.65 (0.10)	1.81 (0.13)	3.21 (0.37)	1.74 (0.13)	⋯

[a] Distances are given in Å. Numbers in parentheses correspond to standard deviations from average values. A maximum distance of 3 Å was chosen as a limit to be considered a hydrogen bond.
[b] See Figure 4 of the main text for conventions on the atom labels.
[c] Two MD simulations were carried out using different initial velocity distribution as indicated by *.
[d] This hydrogen bond is disrupted when the Sub:**O** atom moves toward the oxyanion hole.

Table S5

Lifetime[a] (in ps) of the TI-2 structures of *R*-propranolol during the 1500 ps MD simulations[b].

TI-2[c]	Lifetime	Lifetime*
TI-R1a	1176	1205
TI-R1b	315	286
TI-R2a[d]	71	68
TI-R2b[d]	8	10
TI-R3a	926	96
TI-R3b	564	1394
TI-R4a[e]	148	228
TI-R4b[e]	170	334
TI-R5a[f]	1216	995
TI-R5b[f]	275	495
TI-R6[f]	1490	1490

[a] Lifetime corresponds to the simulation time during which each TI-2 is present.
[b] Two MD simulations with different initial velocity distributions were carried out as indicated by *.
[c] In all MD simulations of TI-2 (except TI-R6) two distinct configurations (a and b) are observed. Configuration a is characterized either by the formation of the Sub:*H*-Thr40:O hydrogen bond (in TI-2 structures in binding mode I) or the Sub:*H*-Sub:O hydrogen bond (in TI-R5; binding mode II). The total lifetime of the TI-2 structures considering only the orientation of the naphthoxy group in the binding pocket is the sum of the lifetimes of the corresponding configurations.
[d] The naphthoxy group is oriented as in TI-R1 after the first 79 ps and 78 ps of the MD simulations with the first and second (*) seed velocity, respectively.
[e] The naphthoxy group is oriented as in TI-R3 after the first 318 ps and 562 ps of the MD simulations with the first and second (*) seed velocity, respectively.
[f] These TI-2 are different from the corresponding starting structures (see section 3.1.2 and Figure S14).

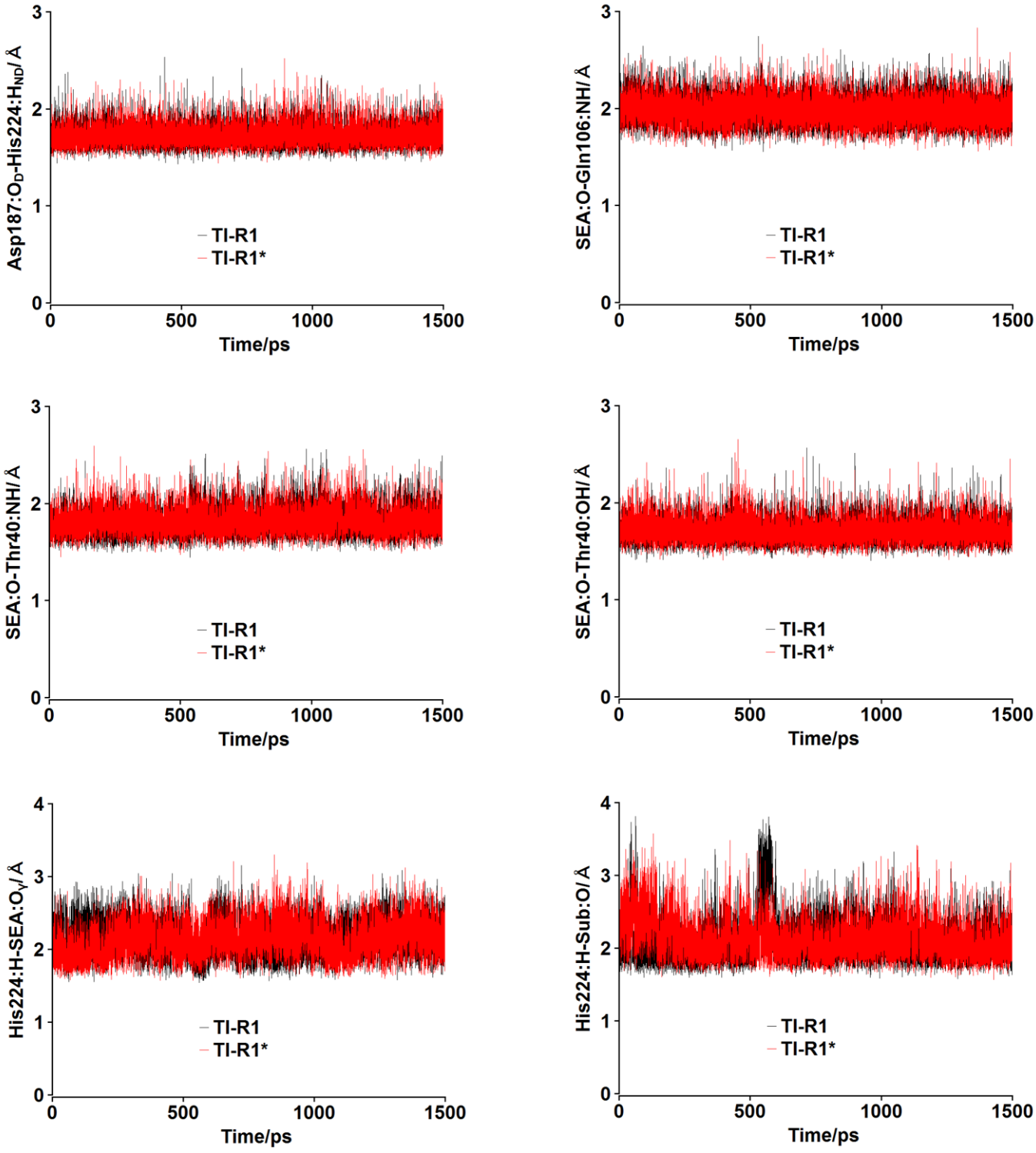

Figure S7. Time evolution of the essential hydrogen bonds for the catalytic activity of CalB in the MD simulations of TI-R1. The simulation with a different initial velocity distribution is indicated by *.

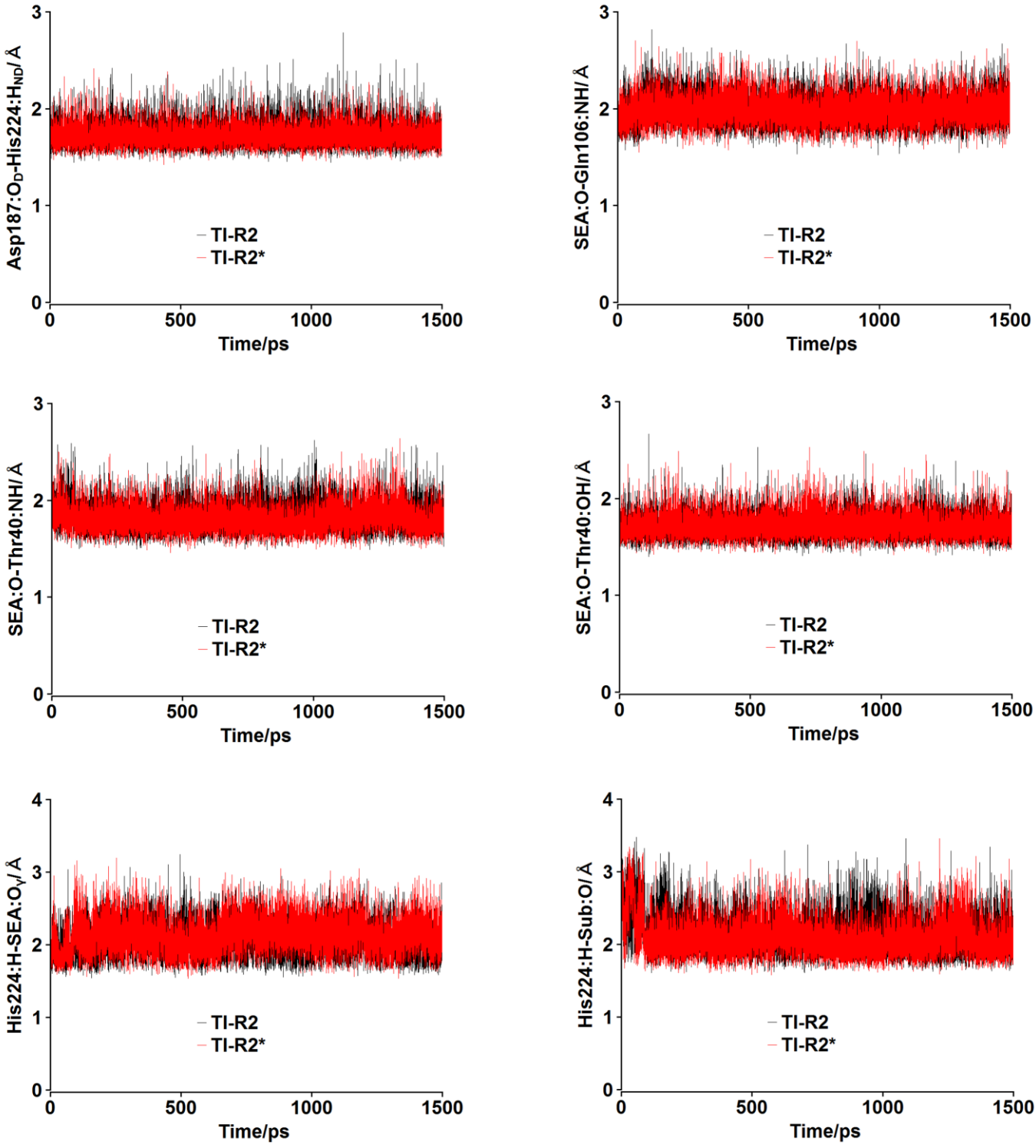

Figure S8. Time evolution of the essential hydrogen bonds for the catalytic activity of CalB in the MD simulations of TI-R2. The simulation with different initial velocity distribution is indicated by *.

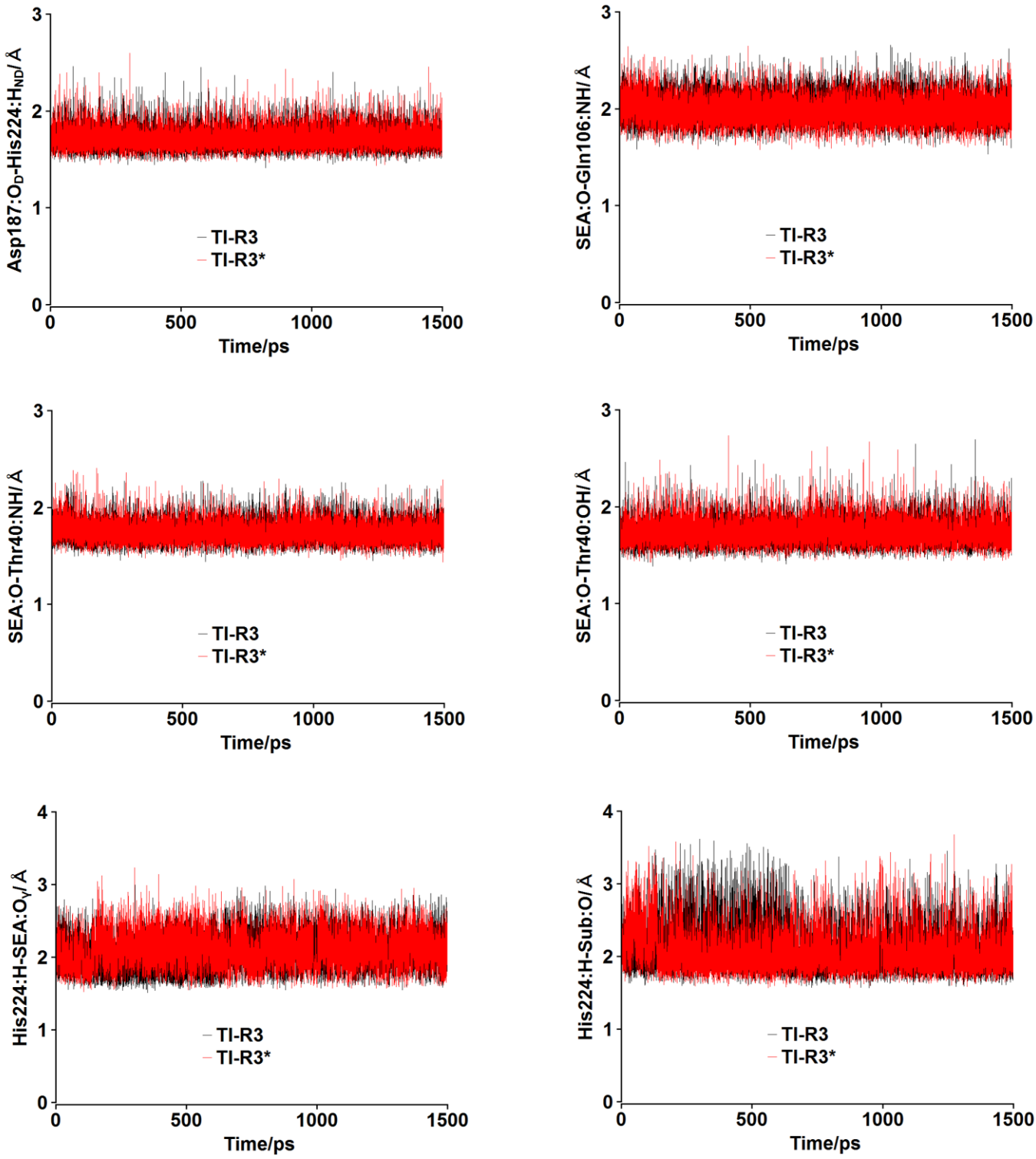

Figure S9. Time evolution of the essential hydrogen bonds for the catalytic activity of CalB in the MD simulations of TI-R3. The simulation with different initial velocity distribution is indicated by *.

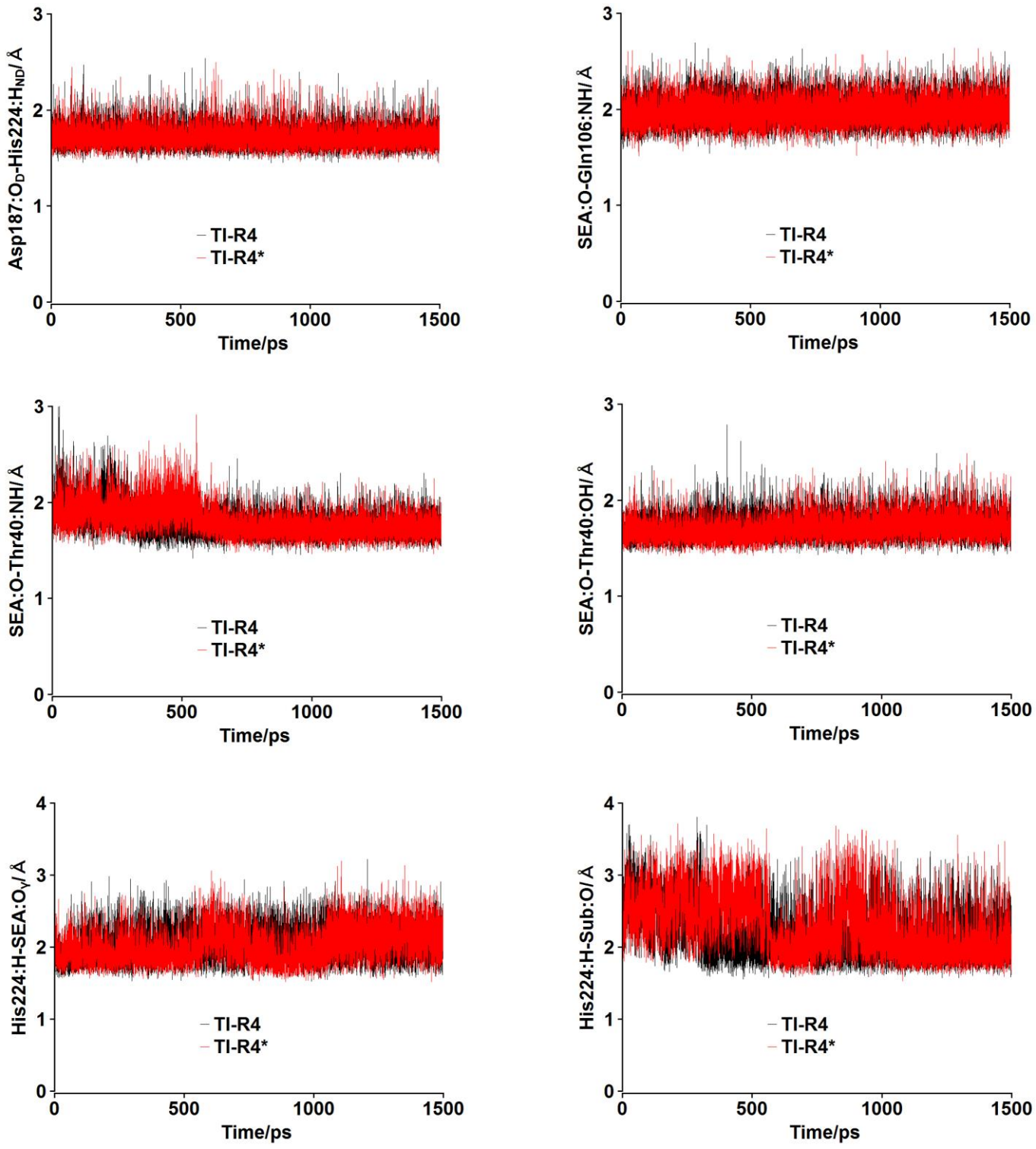

Figure S10. Time evolution of the essential hydrogen bonds for the catalytic activity of CalB in the MD simulations of TI-R4. The simulation with different initial velocity distribution is indicated by *.

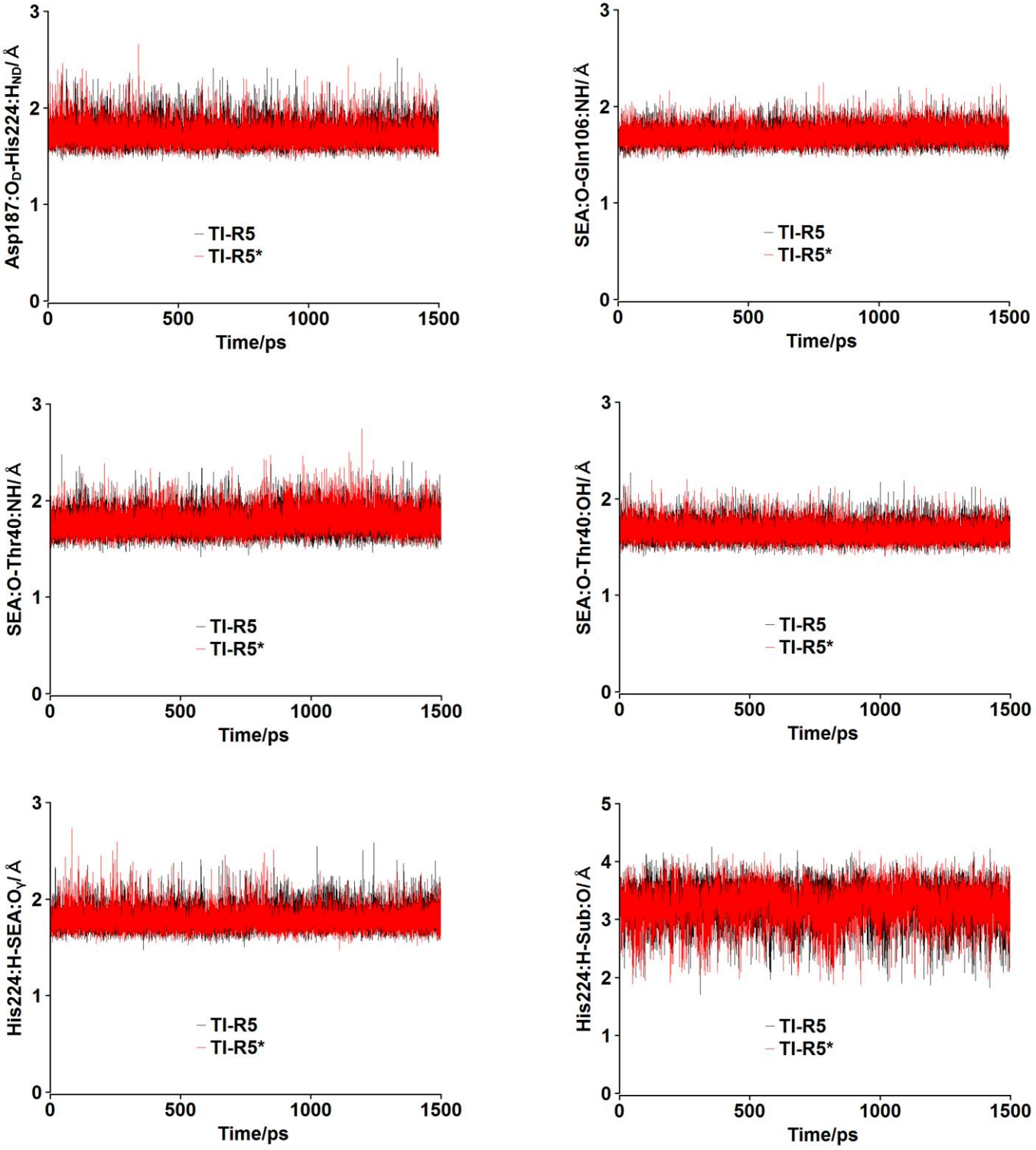

Figure S11. Time evolution of the essential hydrogen bonds for the catalytic activity of CalB in the MD simulations of TI-R5. The simulation with different initial velocity distribution is indicated by *. The movement of the Sub:**O** atom toward the oxyanion hole leads to the disruption of the His224:**H**-Sub:**O** hydrogen bond.

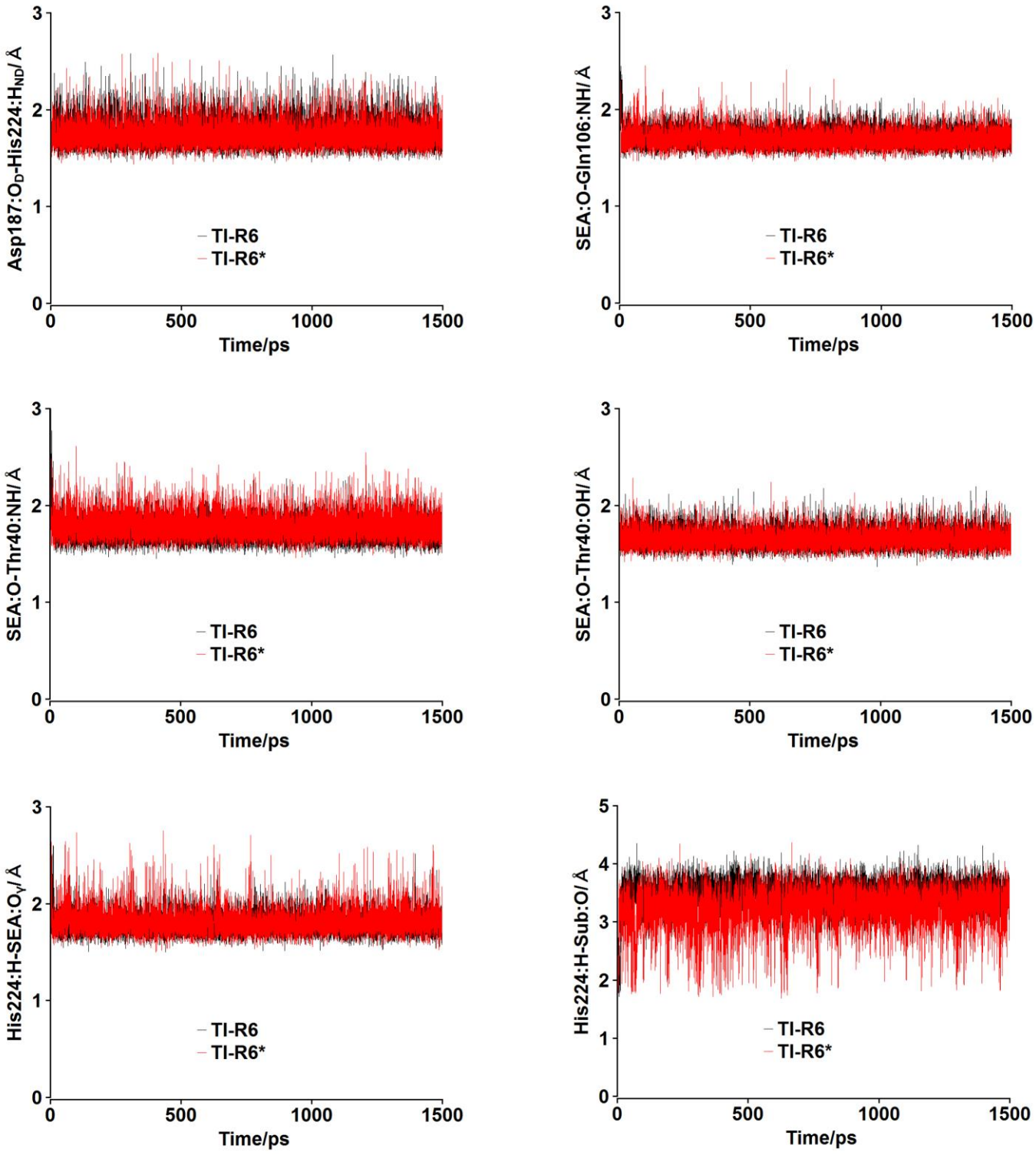

Figure S12. Time evolution of the essential hydrogen bonds for the catalytic activity of CalB in the MD simulations of TI-R6. The simulation with different initial velocity distribution is indicated by *. The movement of the Sub:**O** atom toward the oxyanion hole leads to the disruption of the His224:**H**-Sub:**O** hydrogen bond.

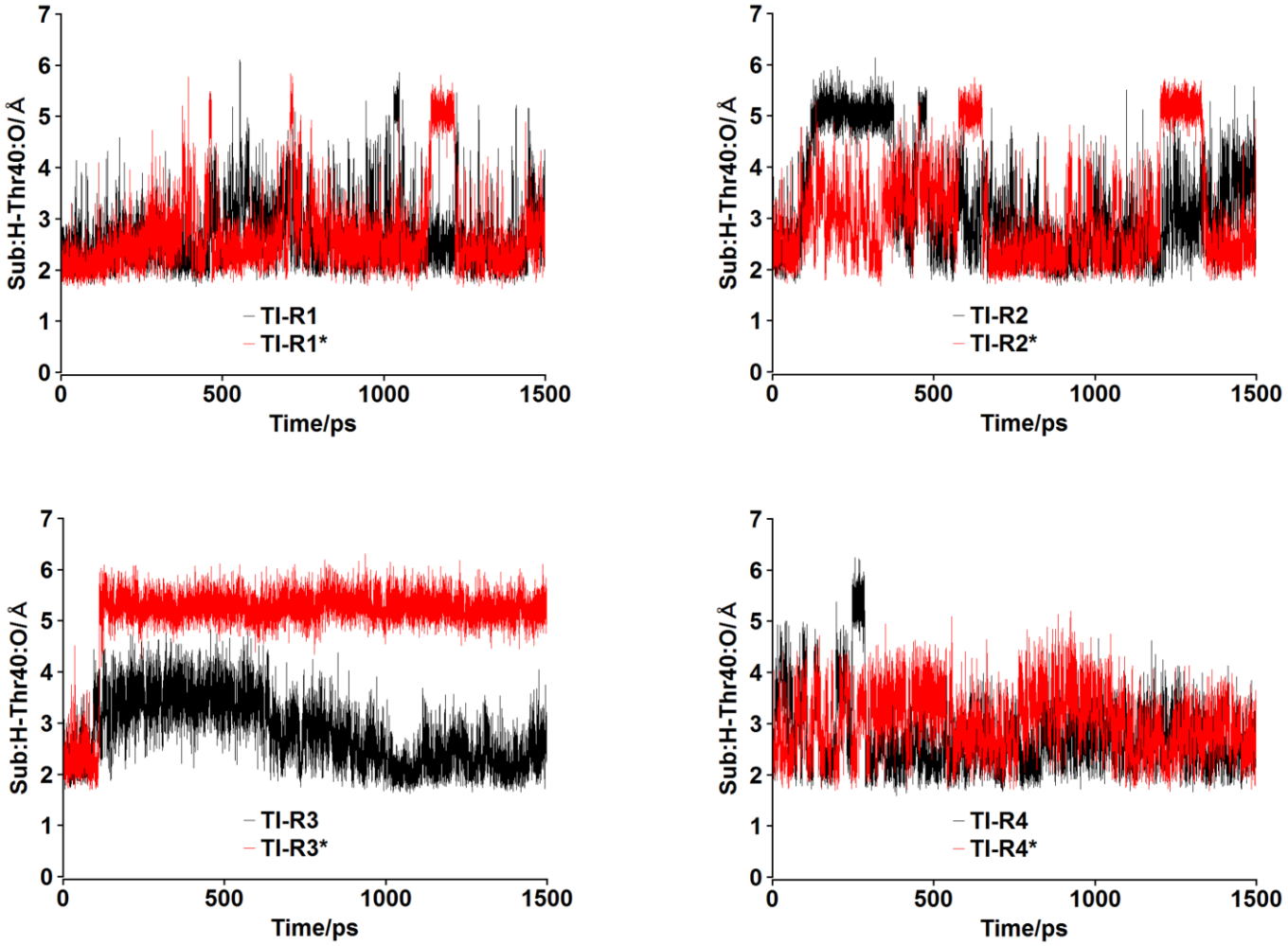

Figure S13. Time evolution of the Sub:*H*-Thr40:O hydrogen bond in the MD simulations of the TI-2 structures of *R*-propranolol in binding mode I. The simulation with different initial velocity distribution is indicated by *. The Sub:*H*-Thr40:O hydrogen bond is formed during 1176 ps, 1205 ps, 778 ps, 862 ps, 926 ps, 96 ps, 1113 ps and 750 ps in the MD simulations of TI-R1, TI-R1*, TI-R2, TI-R2*, TI-R3, TI-R3*, TI-R4 and TI-R4*, respectively.

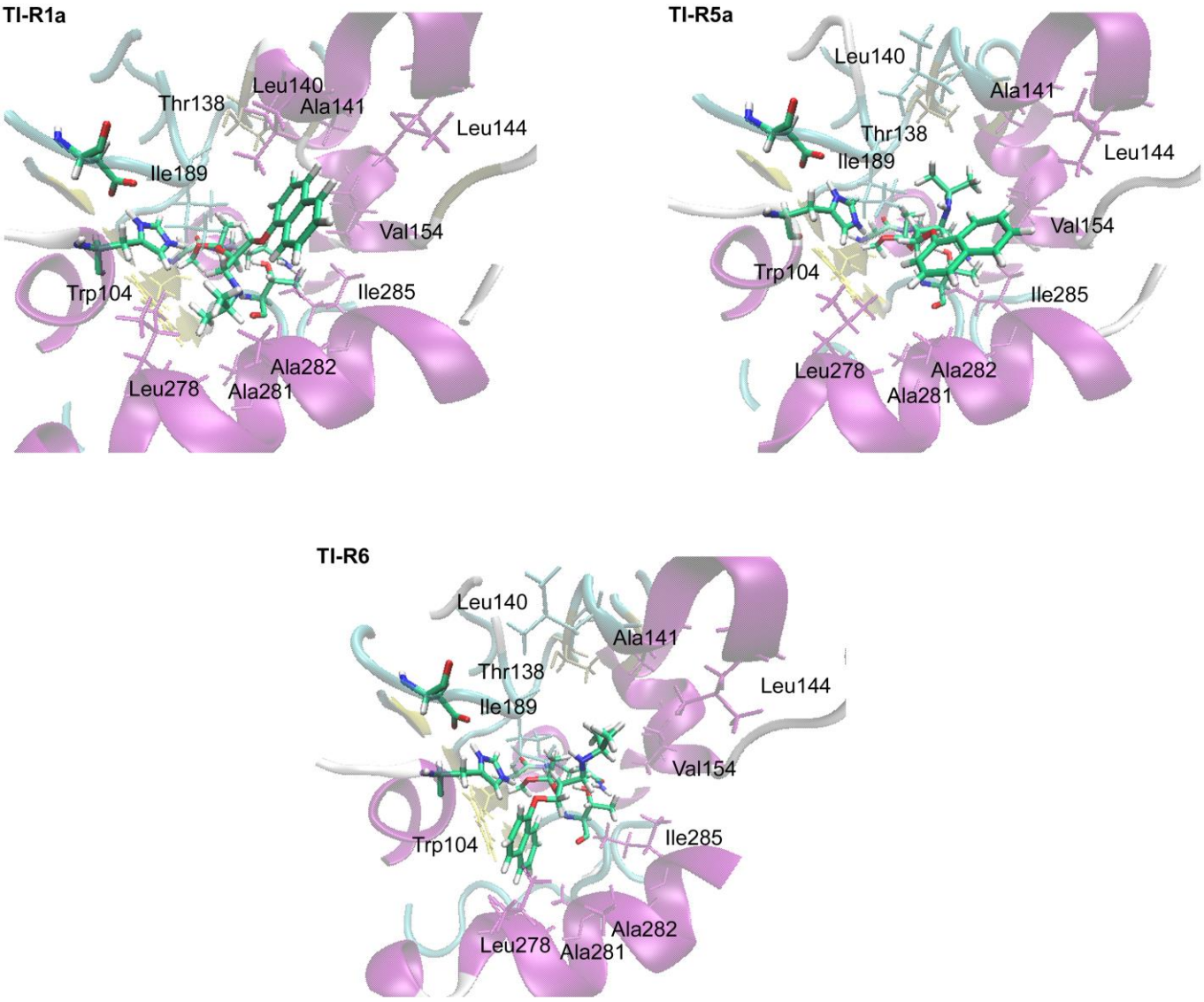

Figure S14. Most dominant structures in the MD simulations of TI-R1, TI-R5 and TI-R6. These structures are different from the starting structures. In the MD simulations of TI-R1 the residue Leu140 is reoriented establishing a stronger CH-π interaction with the naphthyl ring of propranolol. In the MD simulations of TI-R5 the naphthoxy group of propranolol is displaced toward the entrance of the binding pocket. Finally, in the MD simulations of TI-R6 this group is displaced toward the interior of the binding pocket. Furthermore, the Sub:**O** atom is displaced toward the oxyanion hole in the MD simulations of TI-R5 and TI-R6.

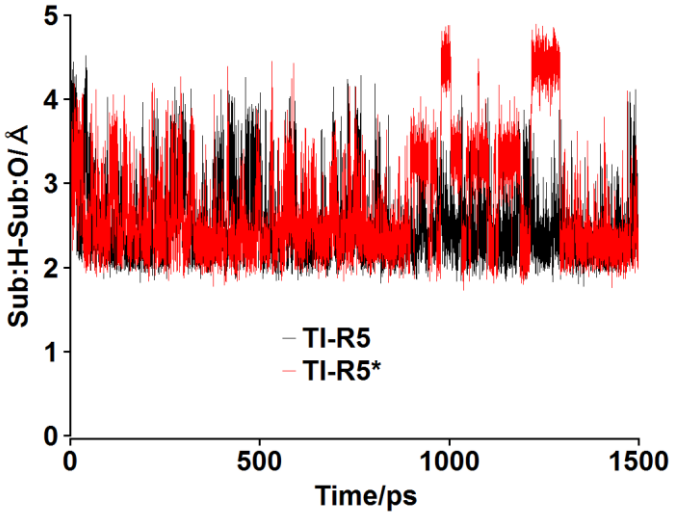

Figure S15. Time evolution of the intramolecular hydrogen bond between the amino and naphthoxy groups of propranolol (Sub:*H*-Sub:O) in the MD simulations of TI-R5. The simulation with different initial velocity distribution is indicated by *. This hydrogen bond is formed during 1216 ps and 995 ps in the MD simulations of TI-R5 and TI-R5*, respectively.

3.2. Analysis of the MD simulations of the TI-2 structures of *S*-propranolol

3.2.1. Stability of the essential hydrogen bonds for the catalytic process in the MD simulations of the TI-2 structures of S-propranolol

The time evolution of the essential hydrogen bonds for the catalytic process in the MD simulations of *S*-propranolol is shown in Figures S16-S21. As observed for *R*-propranolol, the hydrogen bond between Asp187 and His224 is stable throughout the MD simulations of *S*-propranolol, and has a similar average distance in all MD simulations (1.71-1.73 Å; see Table S6). The hydrogen bonds between the oxyanion and the residues of the oxyanion hole are also stable throughout the MD simulations. Furthermore, the average distance of the SEA:O-Gln106:NH hydrogen bond as well as those of the hydrogen bonds between the protonated His224 and the Sub:**O** and SEA:Oγ atoms are dependent on the movement of the Sub:**O** atom toward the oxyanion hole. However, in contrast to *R*-propranolol, the Sub:**O** atom is not displaced toward the oxyanion hole in the MD simulations of *S*-propranolol in binding mode II but in binding mode I (see Table S6 and Figures S16-S21). This shows that in binding mode I *S*-propranolol has difficulties to adopt an orientation which allows the reaction to proceed [6,7]. In addition, in the MD simulations of some TI-2 structures in binding mode I (TI-S1 and TI-S3) the displacement of the Sub:**O** atom is observed only after more than 45 ps, and not from the beginning of the production phase (after 10 ps) as observed in the MD simulations of *R*-propranolol in binding mode II. Thus in the MD simulations of TI-S1 and TI-S3 two major configurations are clearly visible, one in which the His224:**H**-Sub:**O** hydrogen bond is formed (configuration i: TI-S[1 or 3]i) and one in which is disrupted due to the displacement of the Sub:**O** atom toward the oxyanion hole (configuration ii: TI-S [1 or 3]ii). In the MD simulations of TI-S3 and of TI-S1 with the second seed velocity, the configuration i (TI-S3i and TI-S1i, respectively) is stable during less than 190 ps after which the configuration ii (TI-S3ii and TI-S1ii, respectively) is formed. In contrast, in the MD simulation of TI-S1 with the first seed velocity, TI-S1i is stable during 1360 ps and then TI-S1ii is formed (see Table S7 and Figures S16 and S18). In the MD simulations of TI-S2 and TI-S4 the configuration ii predominates throughout the trajectories (see Figures S17 and S19), and it is thus expected that among all TI-2 structures of *S*-propranolol in binding mode I the transformation of TI-S1 will be favored.

3.2.2. Dynamic behavior of S-propranolol throughout the MD simulations of TI-2

As observed for *R*-propranolol, the orientation of the isopropylamine side chain of *S*-propranolol is continuously changing in the MD simulations by rotation of the ω_5 dihedral angle. This leads to the temporal formation of the Sub:*H*-Thr40:O hydrogen bond in the MD simulations of *S*-propranolol in binding mode I (see Figure S22), resulting in two major configurations: configuration **a** (TI-S[number]a, this hydrogen bond is formed) and configuration **b** (TI-S[number]b, the hydrogen bond is absent). As shown in Table S7, configuration **b** is more persistent than configuration **a** in almost all MD simulations for *S*-propranolol in binding mode I, which suggests that *R*-propranolol has a higher ability than *S*-propranolol to form the Sub:*H*-Thr40:O hydrogen bond (see also Figures S13 and S22). There are only two particular cases in which this is not observed: (1) the MD simulation of

TI-S1 with the first initial velocity distribution, in which configuration TI-S1ia (with the His224:**H**-Sub:**O** hydrogen bond interaction–see the previous section) is present more frequently (1286 ps) than TI-S1ib (74 ps); (2) the MD simulation of TI-S4 with the second initial velocity distribution, in which the configuration TI-S4iia is found more often (333 ps) than TI-S4iib (257 ps). Considering only the orientation of the naphthoxy group of propranolol in the large pocket of CalB, TI-S1 and TI-S3 are preferred over TI-S2. The naphthoxy group preserves its initial orientation throughout the MD simulations of TI-S1 and TI-S3, while in the MD simulations of TI-S2 it adopts the orientation observed in TI-S1 after less than 90 ps. This group also preserves its initial orientation throughout the MD simulation of TI-S4 with the first seed velocity, whereas in the MD simulation with the second initial velocity distribution it adopts the orientation observed in TI-S1 after 590 ps (see Table S7). Interestingly, when TI-S1 is formed in the MD simulations of TI-S2 and TI-S4, the Sub:**O** atom remains displaced toward the oxyanion hole (configuration ii) throughout the MD simulations (more than 60 % of the time; see Figures S17 and S19). This shows that in binding mode I the preferred configuration of the TI-2 structures of *S*-propranolol is in fact configuration ii, even though in the MD simulation of TI-S1 with the first initial velocity distribution configuration i is found to be stable during 1360 ps, after which configuration ii is formed (see previous section).

Regarding *S*-propranolol in binding mode II, rotation of the ω_5 dihedral angle results in the temporal formation of an intramolecular hydrogen bond between the amino and naphthoxy groups of propranolol (Sub:*H*-Sub:O) in the MD simulations of TI-S5 (see Figure S23), similar to the behavior observed in the MD simulations of TI-R5 (analogue of TI-S5). Thus two configurations are observed, one in which this hydrogen bond is formed (TI-S5a) and one in which is absent (TI-S5b). However, as shown in Table S7, TI-S5b is found more often (more than 870 ps) than TI-S5a (less than 620 ps). This shows that *R*-propranolol has a higher ability to form this hydrogen bond, as TI-R5a is present more than 900 ps (see Table S5). Meanwhile, in the MD simulations of TI-S6, distinct configurations due to rotation of the ω_5 dihedral angle are not identified. But interestingly, in the MD simulation of TI-S6 with the second seed velocity two configurations are identified due to rotation of the ω_9 dihedral angle of TI-2 (see Figure S1) after 1293 ps (see Table S7). The most dominant structures in the MD simulations of TI-S5 and TI-S6 are shown in Figure S24. They differ from the starting structures by the orientation of the naphthoxy group in the medium pocket of CalB, since during heating and equilibration a structural rearrangement takes place, which is mainly attributed to interactions with the solvent.

Judging from the stability of the essential hydrogen bonds for the catalytic process, the transformation of *S*-propranolol is expected to be favored in binding mode II. Among the complexes with binding mode I, the transformation of TI-S1 is expected to be most facile (see section 3.2.1).

Table S6

Hydrogen bond distances[a] involving the TI-2 structures of *S*-propranolol[b] averaged over the 1.5 ns MD simulations[c].

TI-2	SEA:O-Gln106:NH	SEA:O-Thr40:NH	SEA:O-Thr40:OH	His224:**H**-SEA:O_γ	His224:**H**-Sub:**O**[d]	Asp187:O_D-His224:H_{ND}	Sub:*H*-Thr40:O
TI-S1	2.18 (0.26)	1.94 (0.20)	1.68 (0.11)	1.88 (0.18)	2.48 (0.39)	1.72 (0.12)	2.37 (0.47)
TI-S1*	1.71 (0.14)	1.74 (0.12)	1.66 (0.10)	1.81 (0.14)	3.27 (0.36)	1.72 (0.12)	4.10 (1.47)
TI-S2	1.68 (0.09)	1.72 (0.10)	1.67 (0.10)	1.81 (0.12)	3.27 (0.29)	1.73 (0.12)	2.70 (0.66)
TI-S2*	1.67 (0.08)	1.74 (0.11)	1.66 (0.10)	1.78 (0.10)	3.40 (0.21)	1.71 (0.11)	5.49 (0.42)
TI-S3	1.67 (0.12)	1.71 (0.10)	1.68 (0.10)	1.77 (0.10)	3.51 (0.30)	1.73 (0.13)	5.61 (0.47)
TI-S3*	1.72 (0.20)	1.73 (0.12)	1.68 (0.11)	1.80 (0.17)	3.32 (0.54)	1.72 (0.12)	5.49 (0.82)
TI-S4	1.69 (0.09)	1.74 (0.11)	1.66 (0.10)	1.80 (0.11)	3.50 (0.24)	1.72 (0.11)	3.76 (0.98)
TI-S4*	1.68 (0.08)	1.72 (0.10)	1.66 (0.10)	1.81 (0.11)	3.39 (0.28)	1.71 (0.11)	2.87 (0.77)
TI-S5	2.01 (0.16)	1.86 (0.15)	1.71 (0.13)	1.92 (0.19)	2.08 (0.22)	1.72 (0.12)	⋯
TI-S5*	2.01 (0.15)	1.89 (0.15)	1.72 (0.13)	1.92 (0.19)	1.92 (0.20)	1.72 (0.11)	⋯
TI-S6	2.01 (0.15)	1.77 (0.12)	1.72 (0.13)	2.35 (0.31)	2.06 (0.26)	1.71 (0.11)	⋯
TI-S6*	2.03 (0.17)	1.88 (0.17)	1.70 (0.12)	2.39 (0.32)	2.47 (0.37)	1.73 (0.12)	⋯

[a] Distances are given in Å. Numbers in parentheses correspond to standard deviations from average values. A maximum distance of 3 Å was chosen as a limit to be considered a hydrogen bond.
[b] See Figure 4 of the main text for conventions on the atom labels.
[c] Two MD simulations were carried out using different initial velocity distributions as indicated by *.
[d] This hydrogen bond is disrupted when the Sub:**O** atom moves toward the oxyanion hole.

Table S7

Lifetime[a] (in ps) of the TI-2 structures of *S*-propranolol identified during the 1500 ps MD simulations[b].

TI-2[c]	Lifetime	Lifetime*
TI-S1ia	1286	1
TI-S1ib	74	69
TI-S1iia	61	583
TI-S1iib	69	837
TI-S2iia[d]	1	1
TI-S2iib[d]	76	42
TI-S3ia	3	21
TI-S3ib	32	162
TI-S3iib	1455	1307
TI-S4iia[e]	504	333
TI-S4iib[e]	986	257
TI-S5a[f]	616	492
TI-S5b[f]	874	999
TI-S6i[f]	1490	1283
TI-S6ii[f]	0	207

[a] Lifetime corresponds to the simulation time during which each TI-2 is present.
[b] Two MD simulations with different initial velocity distributions were carried out as indicated by *.
[c] Different configurations of TI-2 are identified throughout the MD simulations. In the TI-2 structures in binding mode I configuration i is characterized by formation of the His224:**H**-Sub:**O** hydrogen bond, while in configuration ii this hydrogen bond is disrupted as the Sub:**O** atom is displaced toward the oxyanion hole. Moreover, configuration a (ia or iia) is characterized by formation of the Sub:*H*-Thr40:O hydrogen bond. Meanwhile, TI-S5a is characterized by formation of the Sub:*H*-Sub:O hydrogen bond. The total lifetime of the TI-2 structures TI-S1 to TI-S5, considering only the orientation of the naphthoxy group of propranolol in the binding pocket, is the sum of the lifetimes of the corresponding configurations. On the other hand, configurations i and ii of TI-S6 differ in the orientation of the naphthoxy group in the medium pocket.
[d] The naphthoxy group is oriented as in TI-S1 after the first 77 ps and 43 ps of the MD simulations with the first and second (*) seed velocity, respectively.
[e] The naphthoxy group is oriented as in TI-S1 after the first 590 ps of the MD simulation with the second seed velocity (*).
[f] These TI-2 are different from the corresponding starting structures (see section 3.2.2 and Figure S24).

3.3. Concerning the origin of the enantioselectivity of CalB

The MD simulations of TI-2 show that in binding mode II *R*-propranolol has difficulties to adopt an orientation in which the reaction may proceed. The same is observed for *S*-propranolol in binding mode I. Therefore, the competing transformations in CalB are expected to involve mainly *R*-propranolol in binding mode I and *S*-propranolol in binding mode II. This already suggests an explanation for the enantioselectivity of the reaction: the transformation of *R*-propranolol should be favored as in binding mode I the amino group of *R*-propranolol is able to form a hydrogen bond with the carbonyl oxygen of Thr40 (Sub:*H*-Thr40:O), which should stabilize the TI-2 structures and the corresponding TSs. Moreover, while the transformation of *S*-propranolol seems possible in binding mode I via TI-S1, the corresponding reaction of *R*-propranolol via TI-R1 is favored because of the better stabilization by the surrounding protein residues through CH-π interactions (see section 2.1). Furthermore, in the MD simulations of TI-R1 the residue Leu140 is reoriented to form a stronger CH-π interaction with the naphthyl group of propranolol (see Figure S14), which is not observed in the MD simulations of TI-S1. Thus a faster transformation of TI-R1 compared to TI-S1 is expected. All this reinforces our previous conclusion that these CH-π interactions are partly responsible for the enantioselectivity of the reaction. Particularly, the residue Ile189 is expected to be a key for the enantioselectivity of the reaction, because of the orientation of its side chain with respect to the naphthyl ring of propranolol, which facilitates the formation of stronger CH-π interactions.

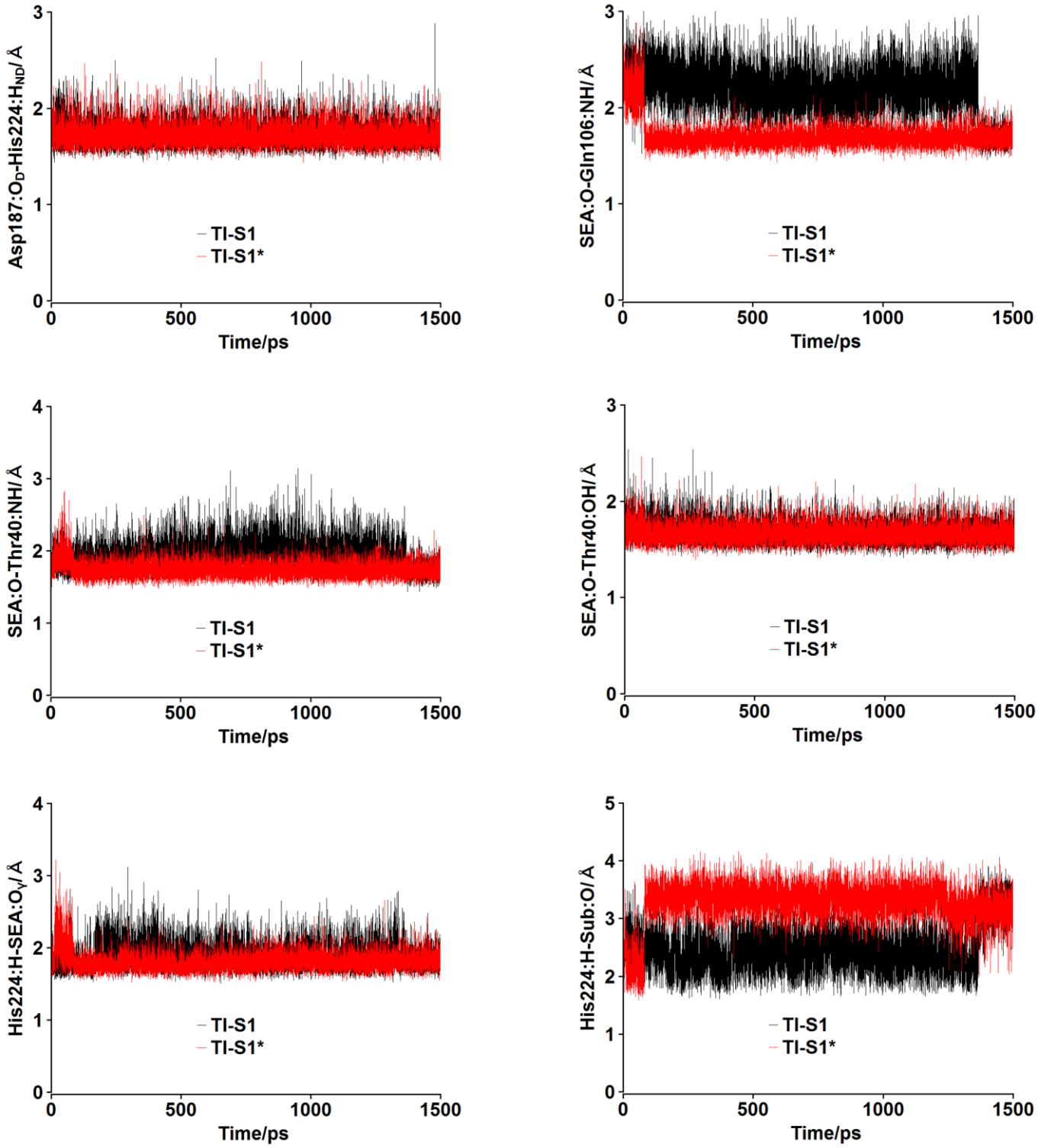

Figure S16. Time evolution of the essential hydrogen bonds for the catalytic activity of CalB in the MD simulations of TI-S1. The simulation with different initial velocity distribution is indicated by *. The movement of the Sub:**O** atom toward the oxyanion hole leads to a disruption of the His224:**H**-Sub:**O** hydrogen bond.

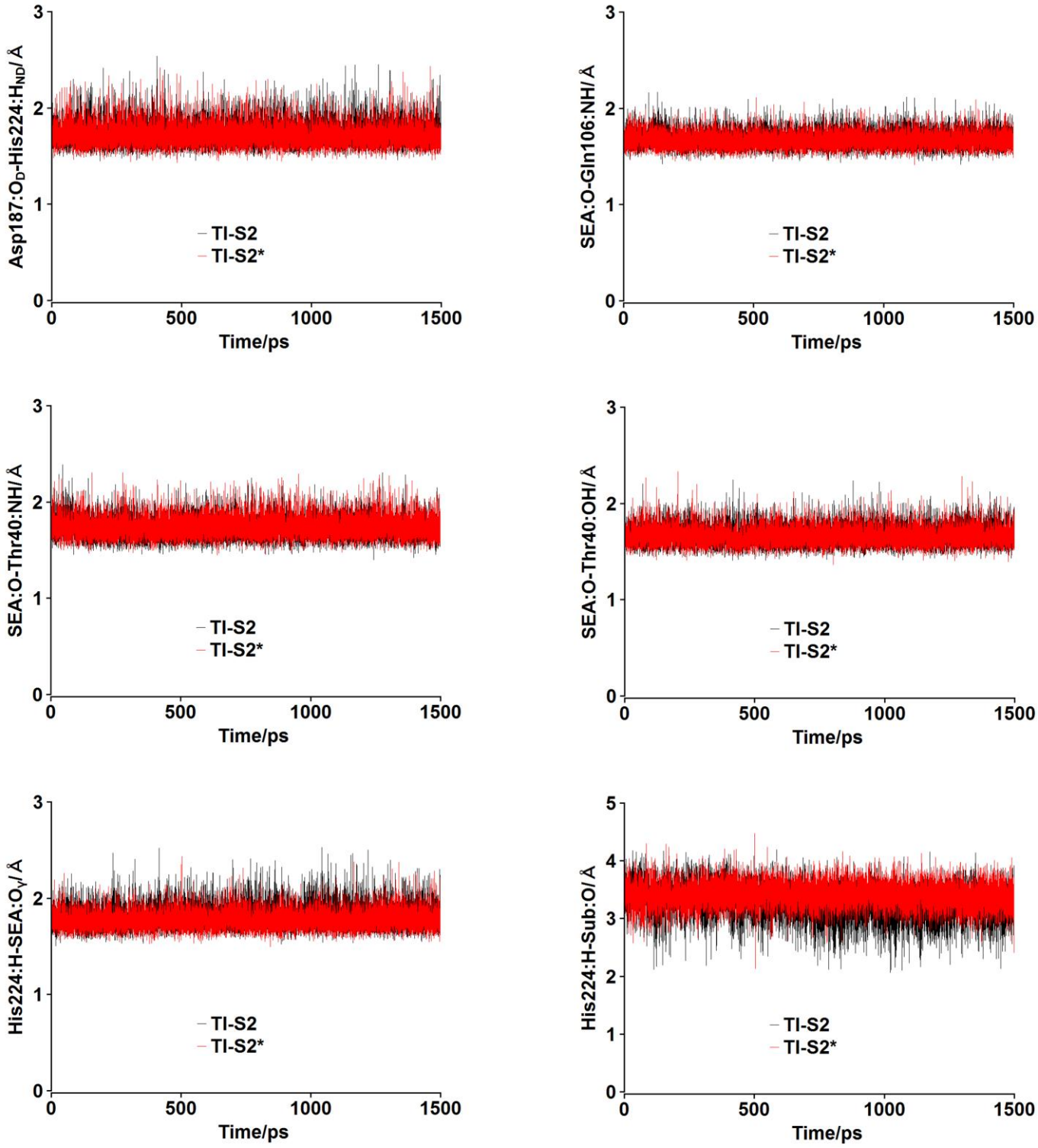

Figure S17. Time evolution of the essential hydrogen bonds for the catalytic activity of CalB in the MD simulations of TI-S2. The simulation with different initial velocity distribution is indicated by *. The movement of the Sub:**O** atom toward the oxyanion hole leads to a disruption of the His224:**H**-Sub:**O** hydrogen bond.

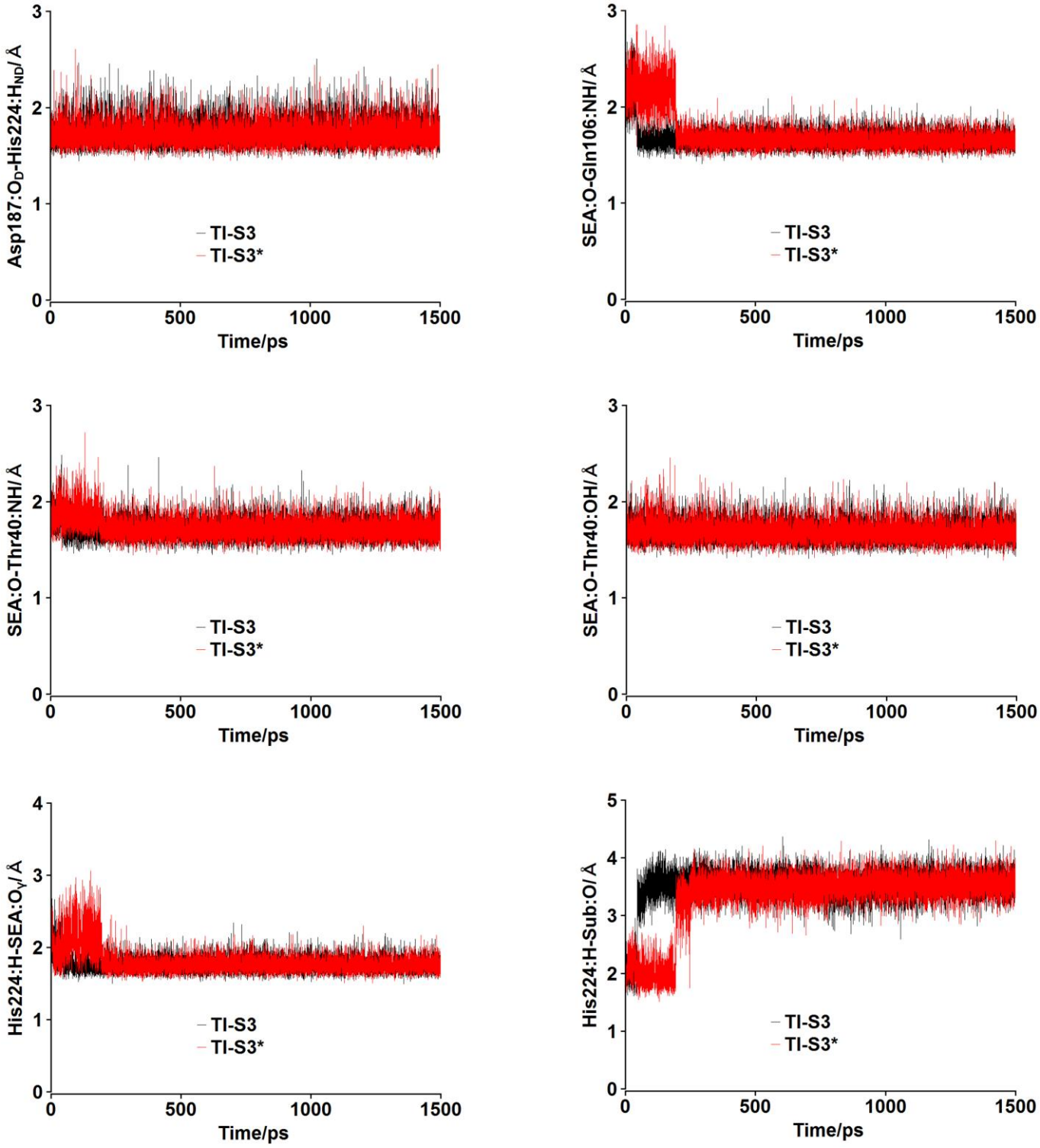

Figure S18. Time evolution of the essential hydrogen bonds for the catalytic activity of CalB in the MD simulations of TI-S3. The simulation with different initial velocity distribution is indicated by *. The movement of the Sub:**O** atom toward the oxyanion hole leads to a disruption of the His224:**H**-Sub:**O** hydrogen bond.

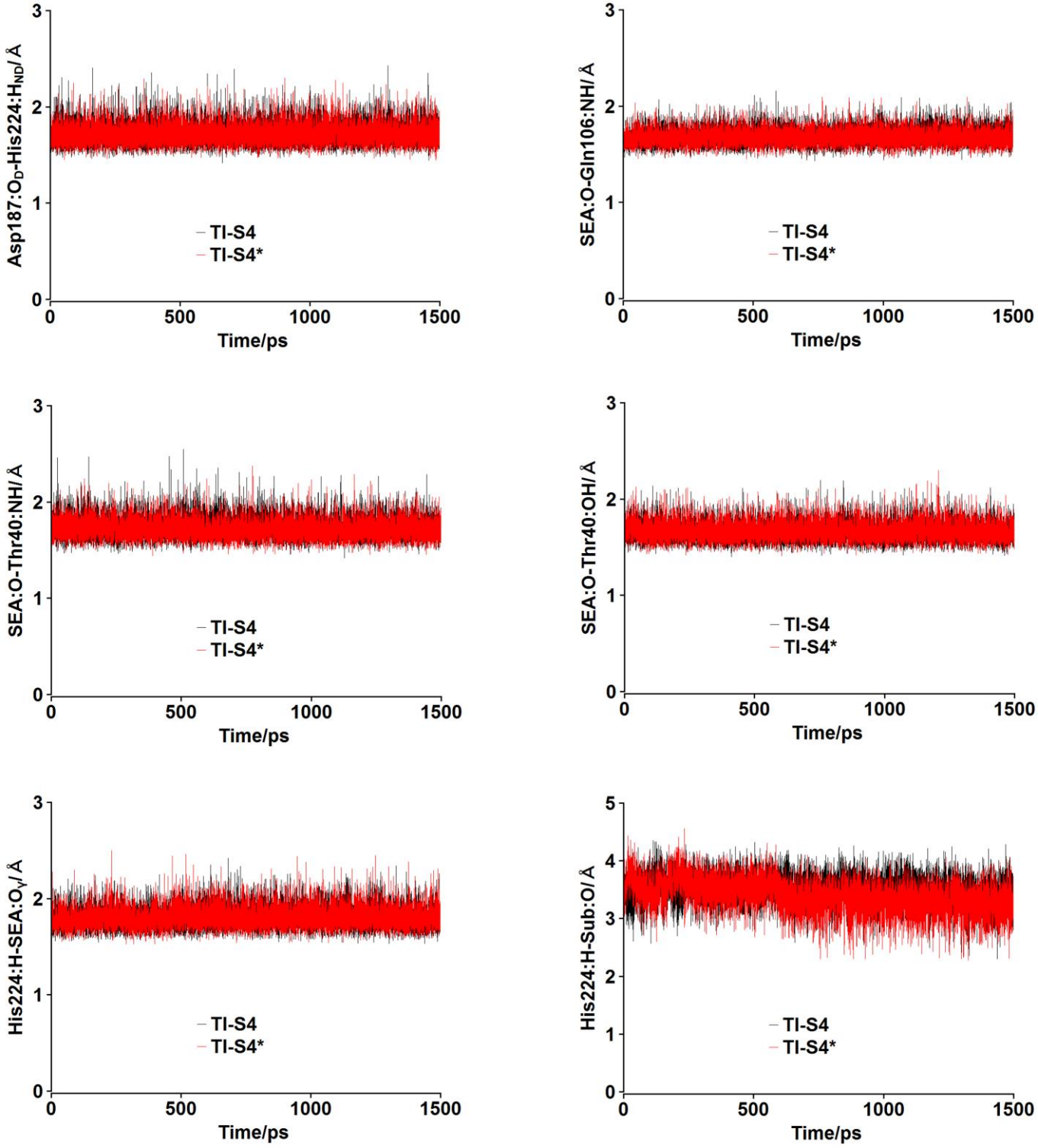

Figure S19. Time evolution of the essential hydrogen bonds for the catalytic activity of CalB in the MD simulations of TI-S4. The simulation with different initial velocity distribution is indicated by *. The movement of the Sub:**O** atom toward the oxyanion hole leads to a disruption of the His224:**H**-Sub:**O** hydrogen bond.

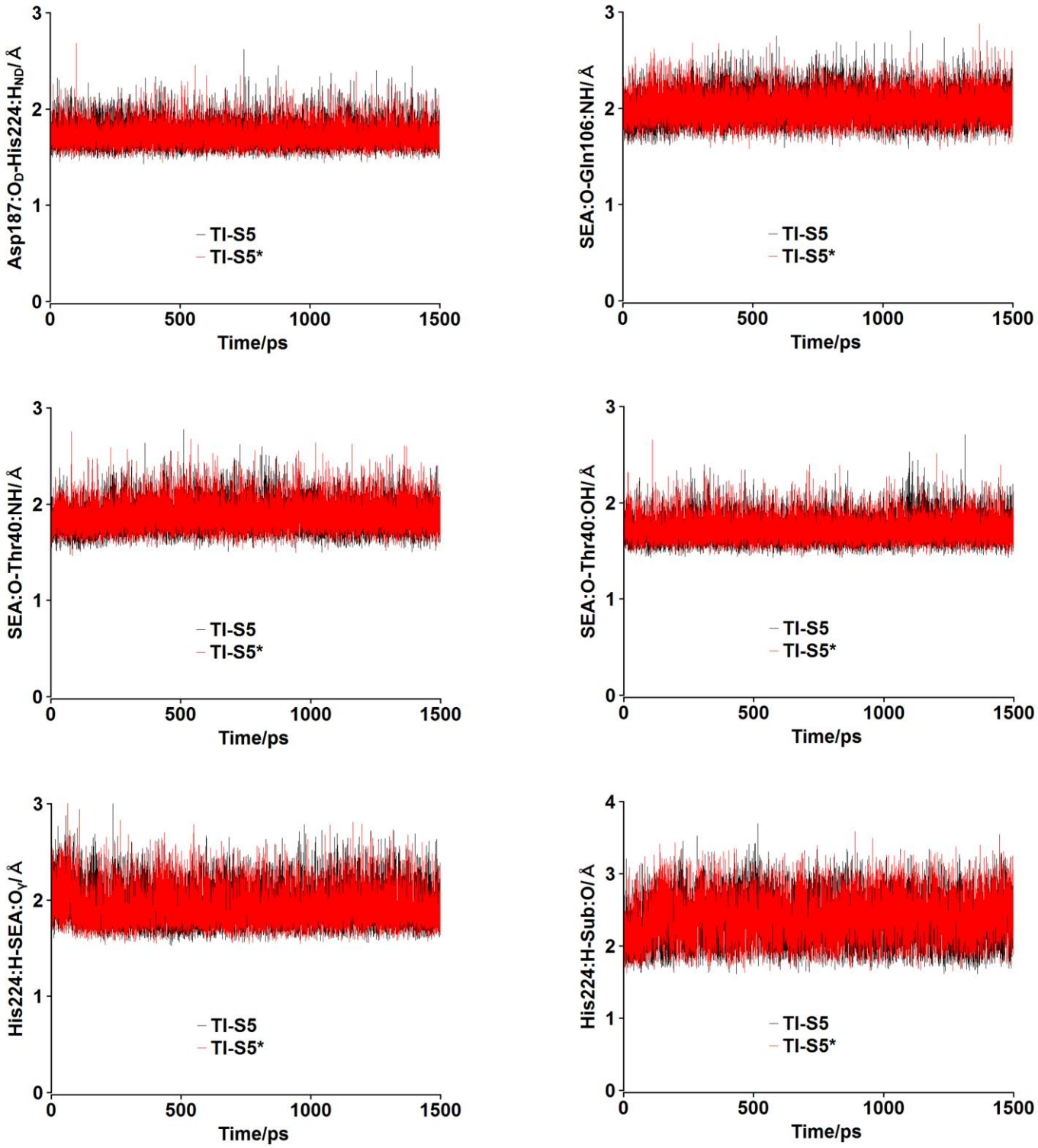

Figure S20. Time evolution of the essential hydrogen bonds for the catalytic activity of CalB in the MD simulations of TI-S5. The simulation with different initial velocity distribution is indicated by *.

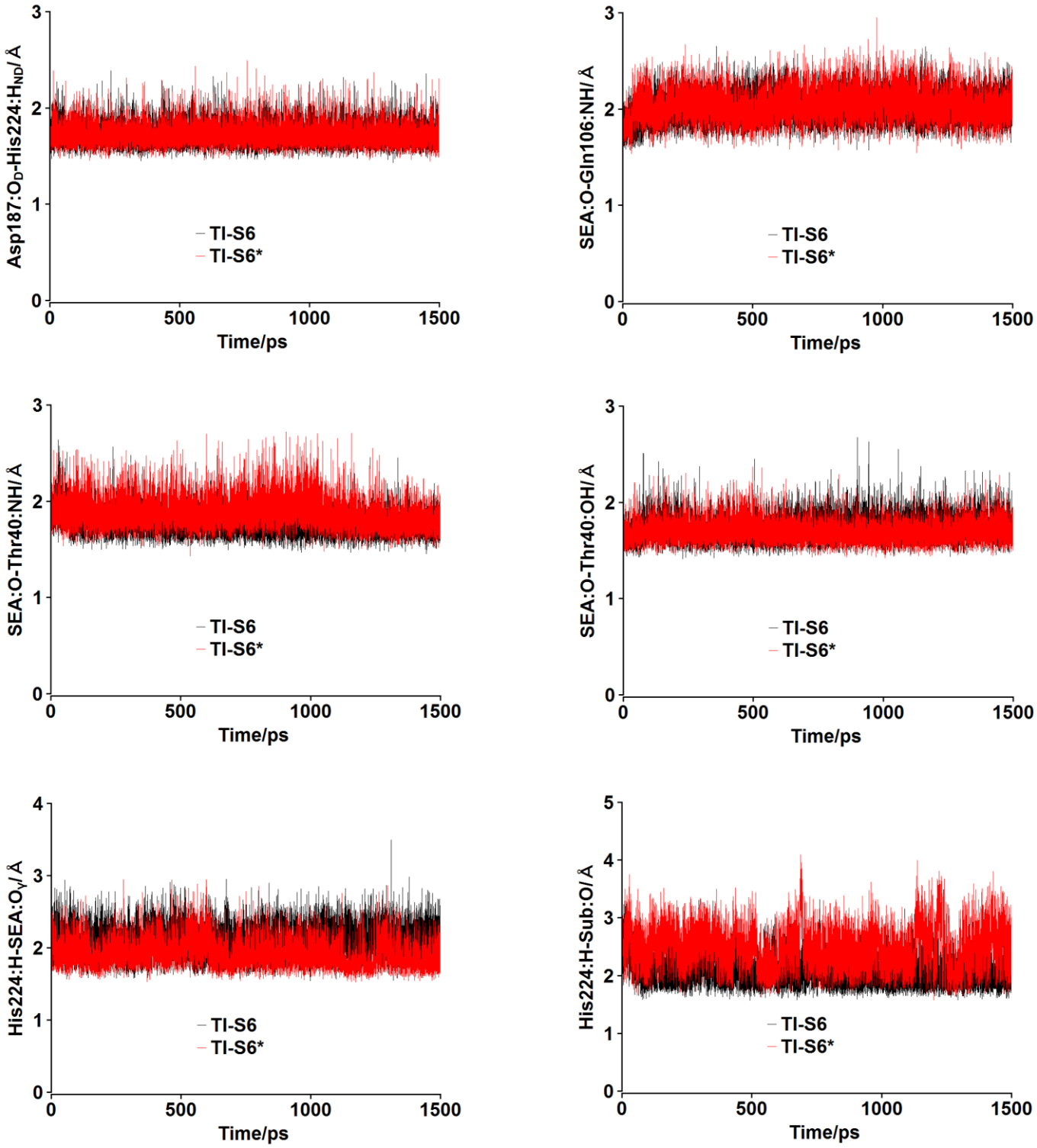

Figure S21. Time evolution of the essential hydrogen bonds for the catalytic activity of CalB in the MD simulations of TI-S6. The simulation with different initial velocity distribution is indicated by *.

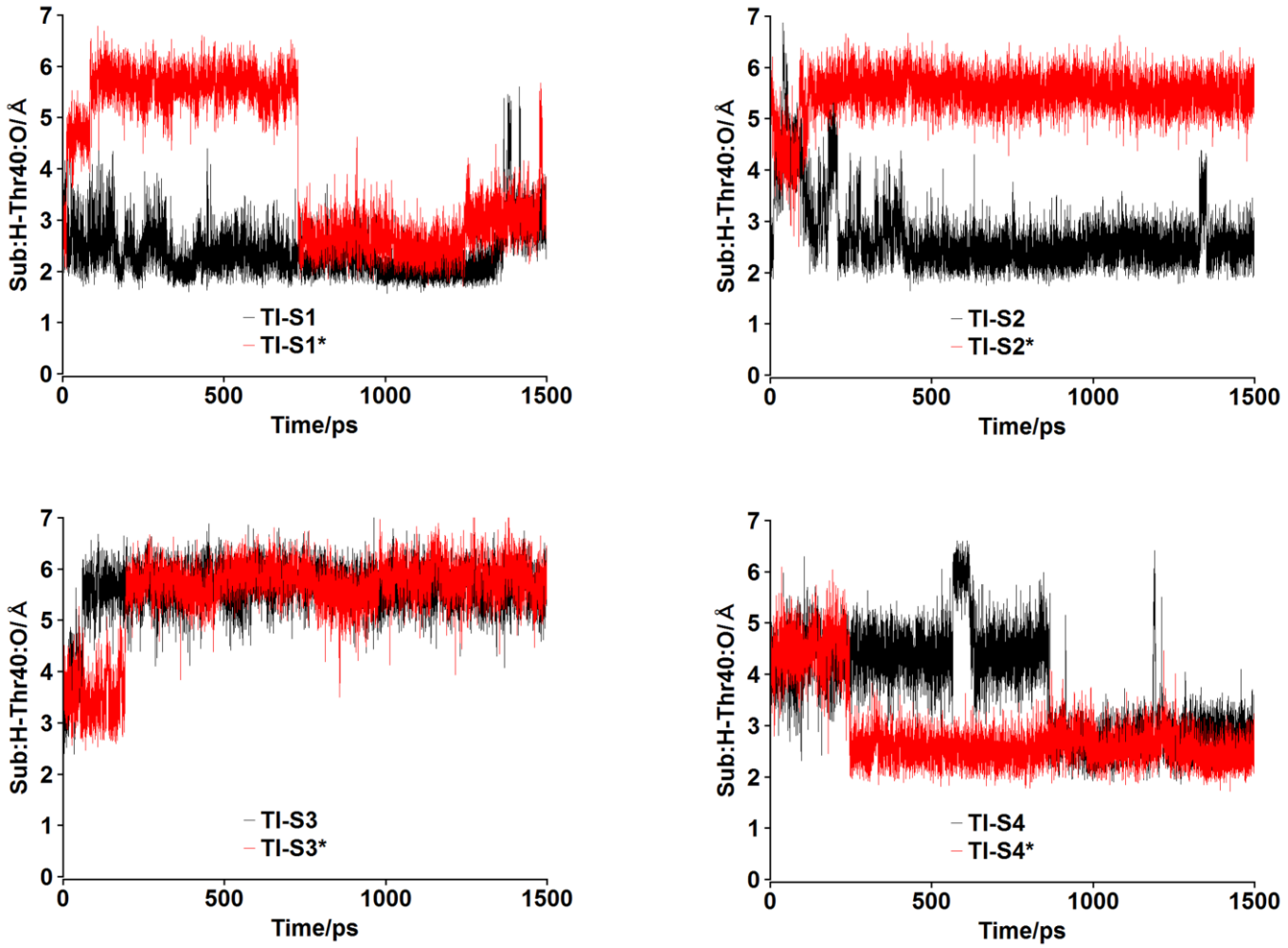

Figure S22. Time evolution of the Sub:*H*-Thr40:O hydrogen bond in the MD simulations of the TI-2 structures of *S*-propranolol in binding mode I. The simulation with different initial velocity distribution is indicated by *. The Sub:*H*-Thr40:O hydrogen bond is formed during 1347 ps, 584 ps, 1226 ps, 1 ps, 3 ps, 21 ps, 504 ps and 1163 ps in the MD simulations of TI-S1, TI-S1*, TI-S2, TI-S2*, TI-S3, TI-S3*, TI-S4 and TI-S4*, respectively.

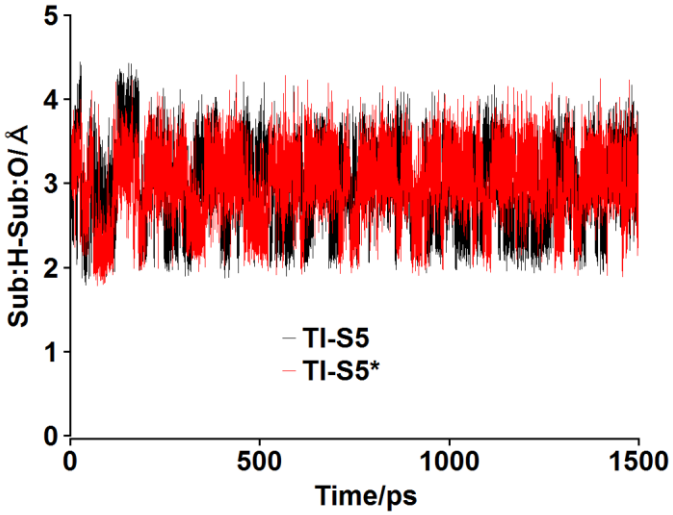

Figure S23. Time evolution of the intramolecular hydrogen bond between the amino and naphthoxy groups of propranolol (Sub:*H*-Sub:O) in the MD simulations of TI-S5. The simulation with different initial velocity distribution is indicated by *. This hydrogen bond is formed during 616 ps and 492 ps in the MD simulations of TI-S5 and TI-S5*, respectively.

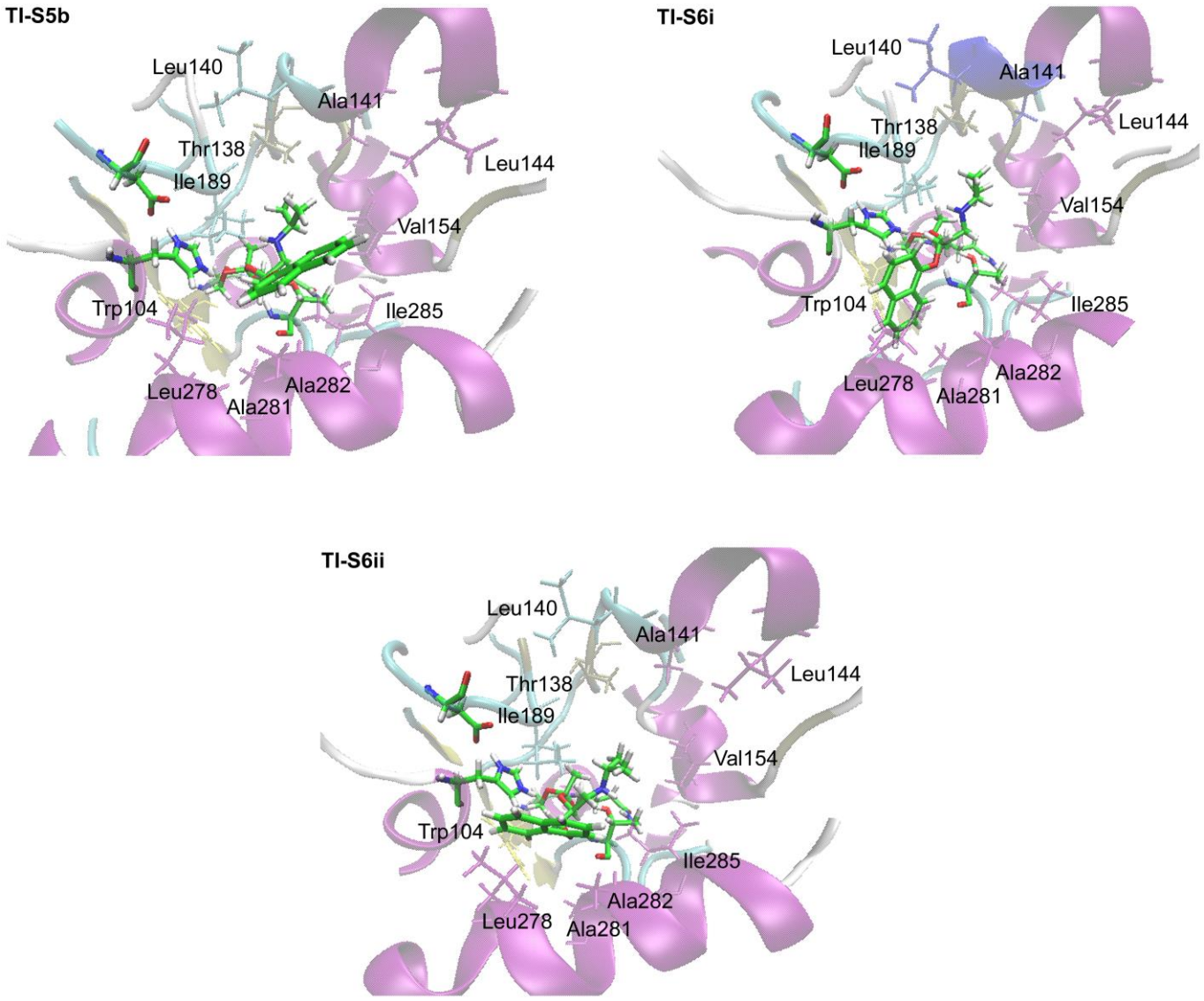

Figure S24. Most dominant structures in the MD simulations of TI-S5 and TI-S6. These structures differ significantly from the starting structures. In the MD simulations of TI-S5 the naphthoxy group of propranolol is oriented parallel to the Leu278-Ala287 helix (helix α10). In the MD simulations of TI-S6 two configurations differing in the orientation of the naphthoxy group in the medium pocket of CalB are identified (TI-S6i and TI-S6 ii). In TI-S6i the naphthoxy group is oriented toward the interior of the pocket. TI-S6ii is generated from TI-S6i by rotation of the ω_9 dihedral angle.

4. QM/MM results

4.1. QM(B3LYP/TZVP)/CHARMM results for the transformation of *R*-propranolol in binding mode I

Table S8

QM(B3LYP/TZVP) and MM(CHARMM) energies in kcal/mol (relative to the MCC) for the transformation of *R*-propranolol in binding mode I via the TI-2 configurations ORI and ORII[a].

Stationary Point	ORI				ORII			
	QM energy		MM energy		QM energy		MM energy	
MCC	0		0		0		0	
TS1	9.4	(9.4)	-2.3	(-2.3)	7.1	(7.1)	-0.6	(-0.6)
TI-2	3.6		-3.1		2.3		0.9	
TS2	6.8	(3.2)	-2.2	(0.9)	6.7	(4.4)	-0.5	(-1.4)
PDC	-1.8		-0.8		0.1		0.8	

[a] Activation barriers relative to the preceding minima are given in parentheses

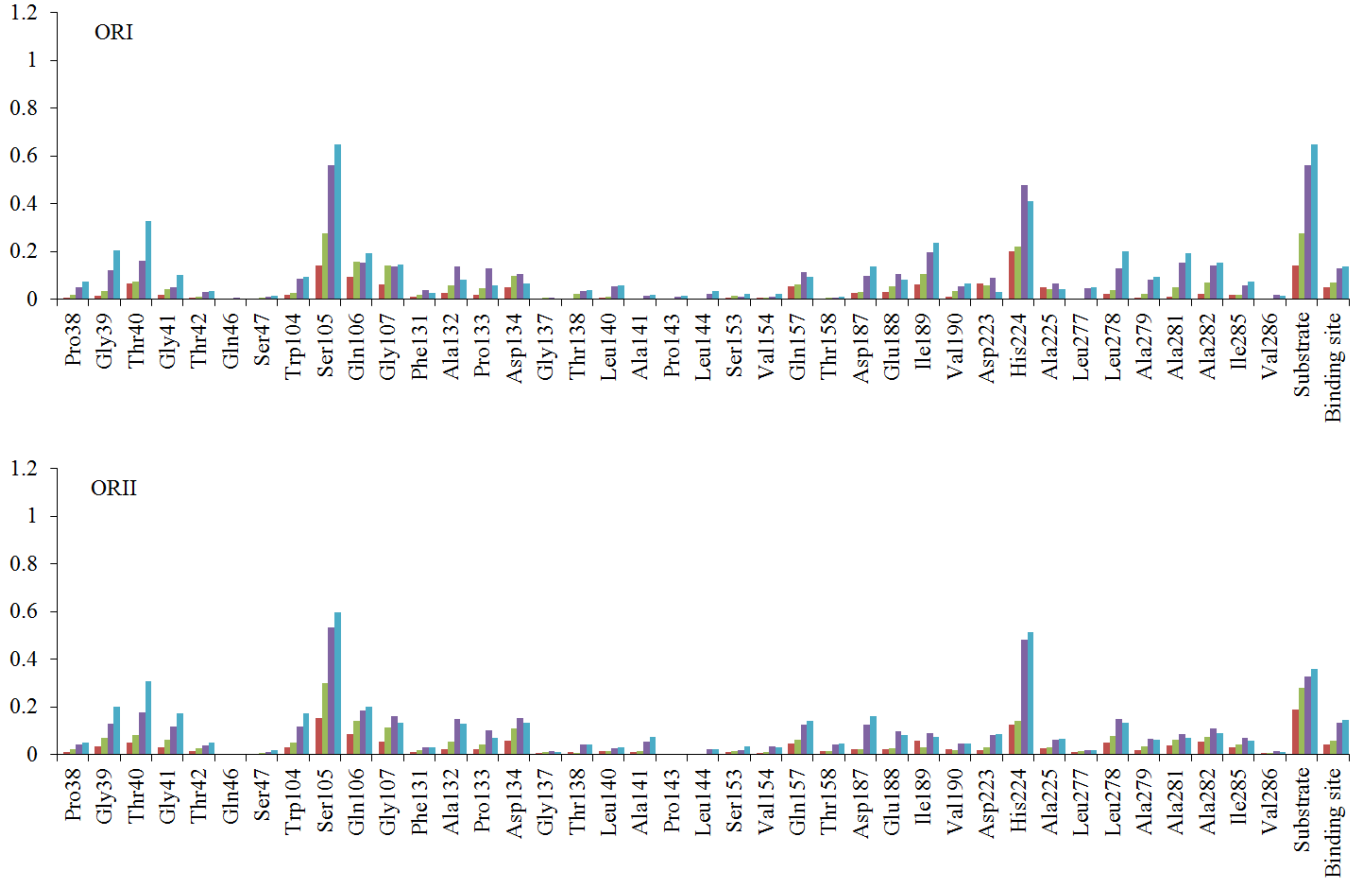

Figure S25. RMSD (in Å, with respect to the MCC) of the residues within 5 Å of the substrate at the stationary points along the reaction profiles of ORI and ORII: TS1 (red), TI-2 (green), TS2 (violet) and PDC (blue). Only heavy atoms were considered. The RMSD for the substrate and the CalB binding site is also shown. The RMSD for the binding site was computed considering all residues within 5 Å of the substrate.

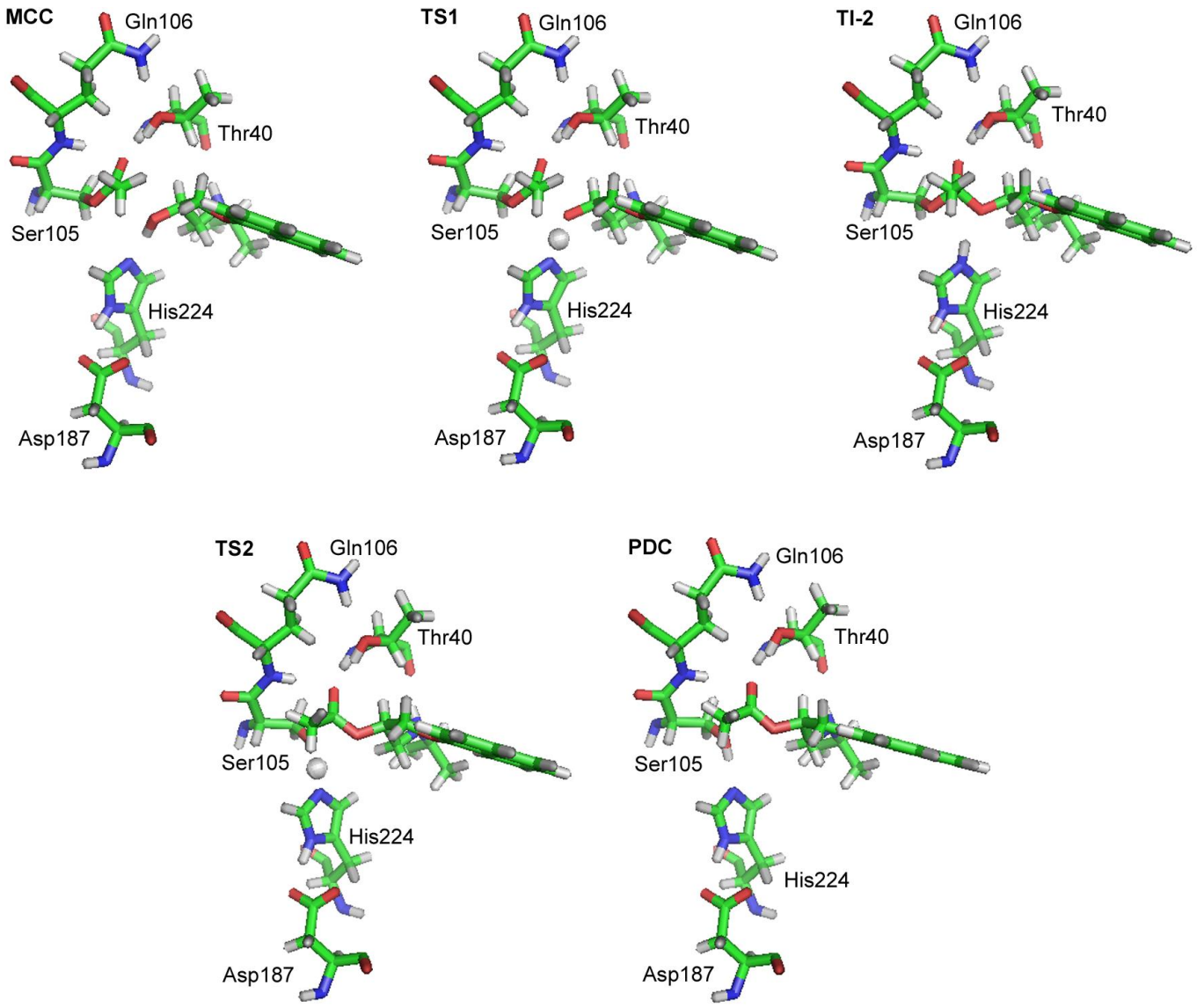

Figure S26. Stationary points along the energy profile for the conversion of *R*-propranolol to *R*-acetyl-propranolol via TI-2 ORI.

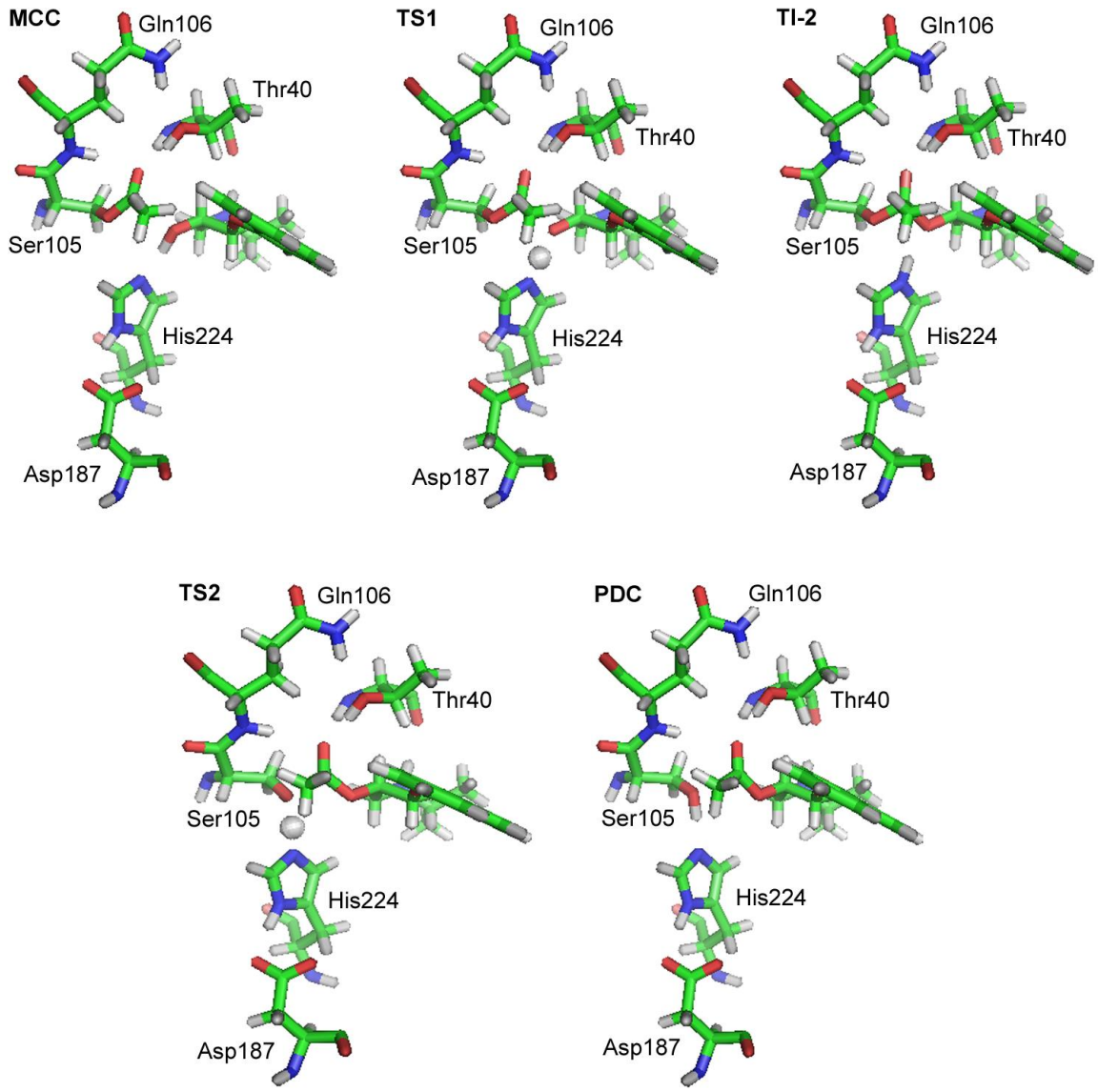

Figure S27. Stationary points along the energy profile for the conversion of *R*-propranolol to *R*-acetyl-propranolol via TI-2 ORII.

Table S9

Distribution of dihedral angles characterizing TI-2[a] at the stationary points along the reaction profiles obtained at the B3LYP(TZVP)/CHARMM level for the transformation of *R*-propranolol in binding mode I via the TI-2 configurations ORI and ORII.

Dihedral (°)	**ORI**					**ORII**				
	MCC	**TS1**	**TI-2**	**TS2**	**PDC**	**MCC**	**TS1**	**TI-2**	**TS2**	**PDC**
ω_1	2	10	15	-20	-26	11	22	32	-3	3
ω_2	30	34	38	6	10	17	24	28	-2	9
ω_3	-148	-150	-151	-122	-114	-117	-124	-128	-102	-110
ω_4	160	159	157	160	154	178	-179	-178	178	177
ω_5	-168	-170	-171	-176	178	94	94	94	95	94
ω_6	63	61	59	61	63	-138	-140	-140	-132	-130
ω_7	120	127	133	136	152	-65	-68	-71	-62	-63
ω_8	-170	-171	-173	-172	-177	172	174	177	168	166
ω_9	-168	-174	-176	-174	-179	-161	-164	-162	-151	-148

[a] ω_1-ω_3 are the dihedral angles directly involved in the formation of TI-2. ω_4-ω_9 are the dihedral angles involving the propranolol molecule. See Figure S1.

Table S10

Relevant interatomic distances and bond angles corresponding to the stationary points along the reaction profiles obtained at the B3LYP(TZVP)/CHARMM level for the transformation of *R*-propranolol in binding mode I via TI-2 configurations ORI and ORII[a].

Distance (Å)	**ORI**					**ORII**				
	MCC	**TS1**	**TI-2**	**TS2**	**PDC**	**MCC**	**TS1**	**TI-2**	**TS2**	**PDC**
Asp187:O_D-His224:H_{ND}	1.74 (169)	1.66 (169)	1.54 (170)	1.57 (174)	1.66 (173)	1.83 (169)	1.75 (168)	1.67 (168)	1.62 (174)	1.69 (175)
His224:**H**-SEA:Oγ	-	-	2.35(129)	1.37 (170)	1.01	-	-	2.40 (123)	1.36 (170)	1.02
SEA:C1-SEA:Oγ	1.34	1.37	1.47	2.01	2.54	1.33	1.37	1.46	1.96	2.43
His224:Nε-His224:**H**	1.83 (164)	1.22 (172)	1.03	1.15 (170)	1.65 (173)	1.71 (168)	1.17 (174)	1.04	1.14 (170)	1.57 (175)
His224:**H**-Sub:**O**	1.00	1.31	1.88 (162)	-	-	1.00	1.34	1.69 (166)	-	-
SEA:C1-Sub:**O**	2.46 (100)	2.07 (105)	1.53 (114)	1.37 (122)	1.33 (124)	2.49 (98)	2.05 (106)	1.56 (114)	1.37 (122)	1.33 (124)
SEA:C1-SEA:O	1.23	1.24	1.29	1.25	1.22	1.23	1.24	1.29	1.25	1.23
SEA:O-Gln106:NH	2.04 (145)	2.00 (154)	1.93 (165)	2.03 (153)	2.35 (141)	2.01 (149)	2.01 (157)	2.00 (166)	2.17 (158)	2.60 (149)
SEA:O-Thr40:NH	1.90 (167)	1.87 (169)	1.79 (170)	1.94 (165)	2.13 (158)	1.87 (172)	1.80 (174)	1.73 (175)	1.76 (171)	1.84 (164)
SEA:O-Thr40:OH	1.71 (173)	1.72 (172)	1.71 (175)	1.73 (174)	1.68 (176)	1.74 (170)	1.74 (170)	1.72 (171)	1.74 (170)	1.69 (169)
Sub:*H*-Thr40:O	1.93 (167)	1.90 (166)	1.87 (167)	1.89 (161)	1.96 (157)	1.93 (163)	1.85 (168)	1.83 (168)	1.90 (174)	1.94 (172)

[a] Distances are given in Å. Angles for the corresponding hydrogen bonds and the nucleophilic attack (Sub:**O**⋯SEA:C1=O) are given in degrees (in parentheses). See Figure 4 of the main text for conventions on the atom labels.

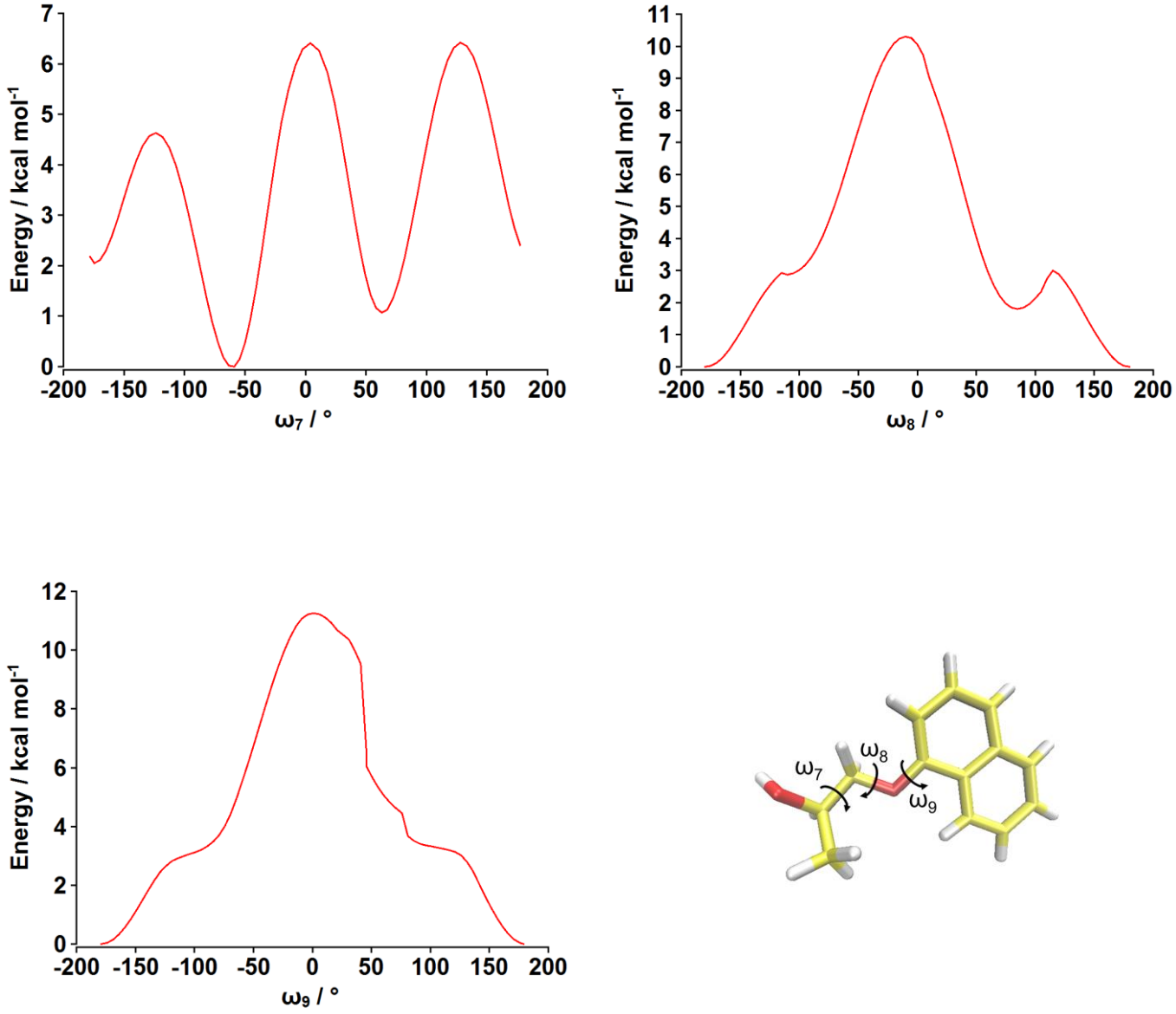

Figure S28. PES scans at the B3LYP/TZVP level along the dihedral angles of *R*-1-methyl-3-(1-naphthoxy)-2-propanol.

4.2. QM(B3LYP/TZVP)/CHARMM results for the transformation of *R*-propranolol in binding mode II

Table S11

QM(B3LYP/TZVP) and MM(CHARMM) energies in kcal/mol (relative to the MCC) for the transformation of *R*-propranolol in binding mode II via the TI-2 configurations ORIII and ORIV[a].

Stationary Point	ORIII				ORIV			
	QM energy		MM energy		QM energy		MM energy	
MCC	0		0		0		0	
TS1	13.3	(13.3)	-3.3	(-3.3)	17.5	(17.5)	-1.3	(-1.3)
TI-2	0.1		-3.9		16.4		-1.7	
TS2	2.0	(1.9)	-3.8	(0.1)	21.6	(5.2)	-3.3	(-1.6)
PDC	-5.7		-3.1		9.7		-1.1	

[a] Activation barriers relative to the preceding minima are given in parentheses

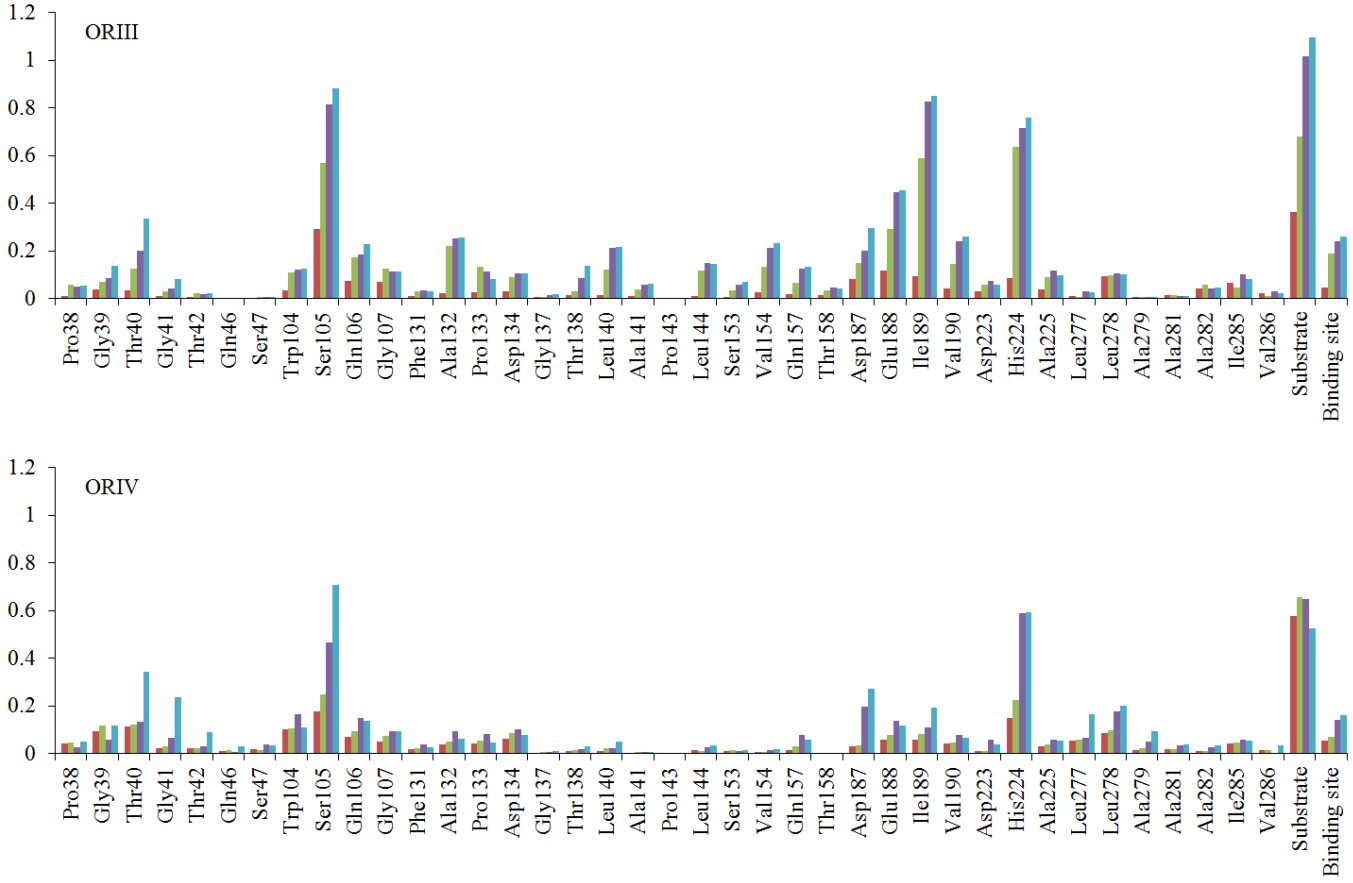

Figure S29. RMSD (in Å, with respect to the MCC) of the residues within 5 Å of the substrate at the stationary points along the reaction profiles of ORIII and ORIV: TS1 (red), TI-2 (green), TS2 (violet) and PDC (blue). Only heavy atoms were considered. The RMSD for the substrate and the CalB binding site is also shown. The RMSD for the binding site was computed considering all residues within 5 Å of the substrate.

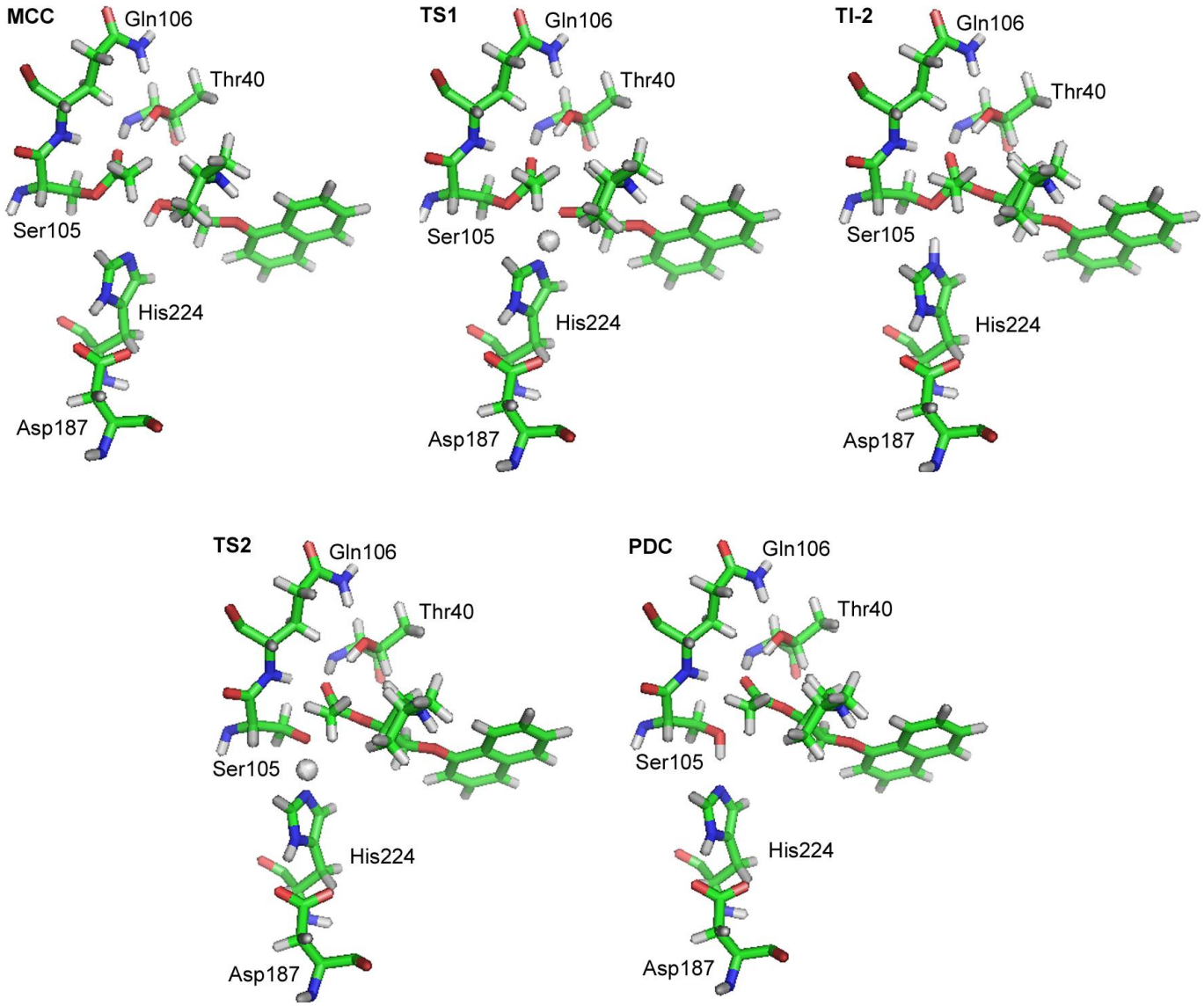

Figure S30. Stationary points along the energy profile for the conversion of *R*-propranolol to *R*-acetyl-propranolol via ORIII. The formation of TI-2 is accompanied by the displacement of the alcohol oxygen toward the oxyanion hole.

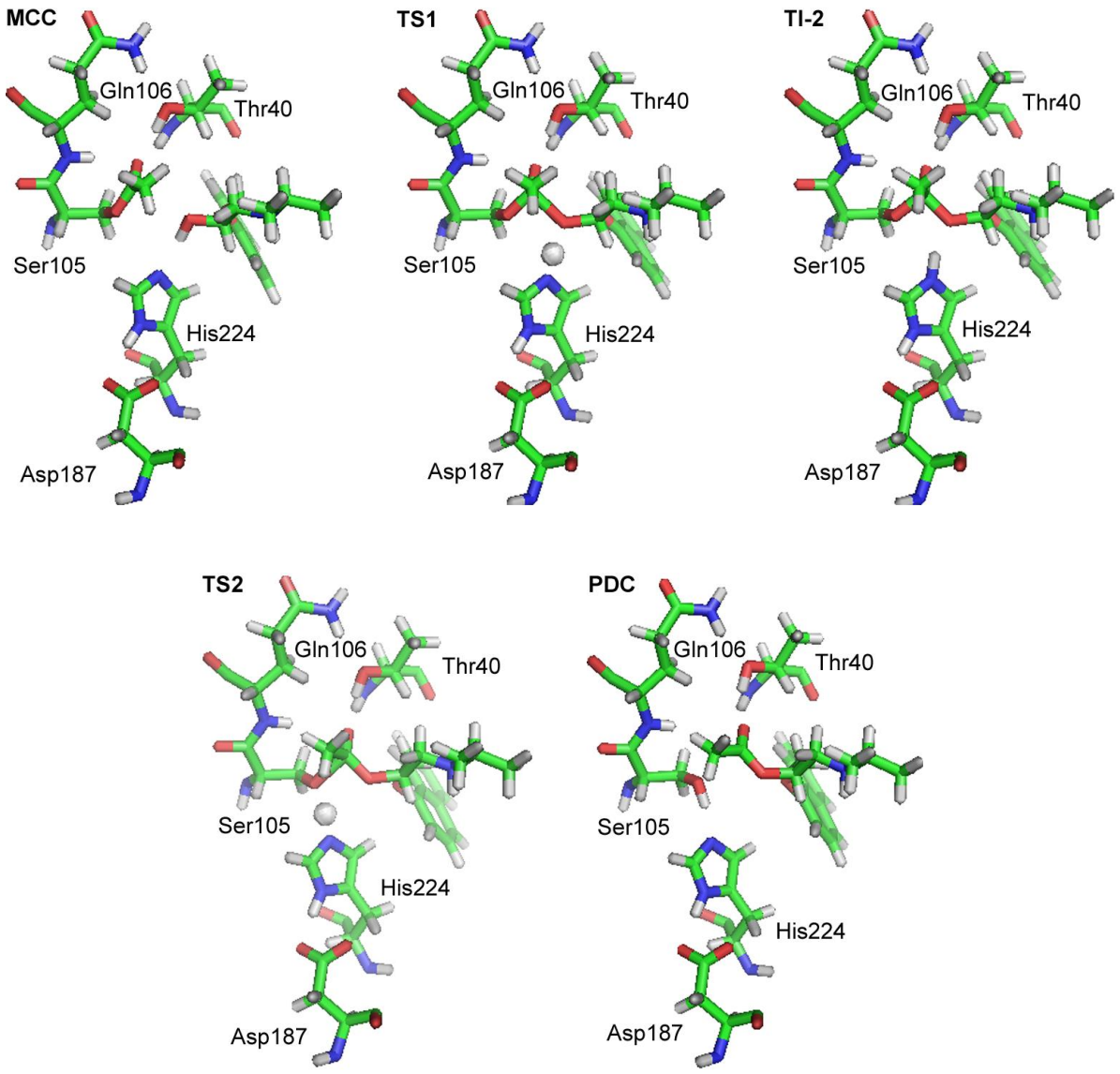

Figure S31. Stationary points along the energy profile for the conversion of *R*-propranolol to *R*-acetyl-propranolol via ORIV.

Table S12

Distribution of dihedral angles characterizing TI-2[a] at the stationary points along the reaction profiles obtained at the B3LYP(TZVP)/CHARMM level for the transformation of *R*-propranolol in binding mode II via the TI-2 configurations ORIII and ORIV.

Dihedral (°)	**ORIII**					**ORIV**				
	MCC	**TS1**	**TI-2**	**TS2**	**PDC**	**MCC**	**TS1**	**TI-2**	**TS2**	**PDC**
ω_1	-13	-13	-12	-8	-6	1	14	19	-8	-11
ω_2	105	89	122	137	159	63	52	52	30	22
ω_3	-46	-32	-69	-71	-79	45	58	59	74	80
ω_4	138	139	153	155	154	171	157	154	147	144
ω_5	-81	-83	-83	-84	-82	176	177	177	-175	-171
ω_6	-155	-155	-147	-151	-150	-178	-176	-176	-177	-175
ω_7	171	176	168	164	159	-47	-55	-55	-57	-57
ω_8	177	172	-179	-171	-168	-100	-100	-103	-118	-114
ω_9	163	167	158	155	153	-146	-134	-129	-101	-110

[a] ω_1-ω_3 are the dihedral angles directly involved in the formation of TI-2. ω_4-ω_9 are the dihedral angles involving the propranolol molecule. See Figure S1.

Table S13

Relevant interatomic distances and bond angles corresponding to the stationary points along the reaction profiles obtained at the B3LYP(TZVP)/CHARMM level for the transformation of *R*-propranolol in binding mode II via the TI-2 configurations ORIII and ORIV[a].

Distance (Å)	**ORIII**					**ORIV**				
	MCC	**TS1**	**TI-2**	**TS2**	**PDC**	**MCC**	**TS1**	**TI-2**	**TS2**	**PDC**
Asp187:O_D-His224:H_{ND}	1.94 (166)	1.82 (166)	1.65 (171)	1.69 (172)	1.76 (174)	1.88 (170)	1.69 (172)	1.63 (172)	1.60 (177)	1.70 (177)
His224:**H**-SEA:Oγ	-	-	1.64 (173)	1.40 (175)	1.02	-	-	2.37 (128)	1.38 (169)	1.01
SEA:C1-SEA:Oγ	1.34	1.38	1.58	1.97	2.49	1.33	1.40	1.48	1.93	2.66
His224:Nε-His224:**H**	1.81 (175)	1.15 (176)	1.05	1.14 (175)	1.58 (176)	1.91 (168)	1.11 (169)	1.05	1.14 (169)	1.66 (171)
His224:**H**-Sub:**O**	1.00	1.43	3.09 (138)	-	-	0.99	1.47	1.69 (161)	-	-
SEA:C1-Sub:**O**	2.61 (96)	2.07 (106)	1.44 (112)	1.38 (114)	1.34 (117)	2.73 (103)	1.87 (112)	1.55 (116)	1.39 (122)	1.33 (124)
SEA:C1-SEA:O	1.22	1.24	1.29	1.25	1.22	1.23	1.25	1.28	1.25	1.22
SEA:O-Gln106:NH	1.98 (146)	1.94 (154)	1.73 (166)	1.77 (160)	1.90 (156)	2.03 (152)	2.18 (163)	2.27 (168)	2.55 (161)	3.19 (152)
SEA:O-Thr40:NH	1.96 (168)	1.99 (168)	1.83 (168)	1.86 (167)	1.89 (165)	2.04 (161)	1.89 (167)	1.85 (168)	1.93 (163)	2.25 (151)
SEA:O-Thr40:OH	1.74 (172)	1.73 (172)	1.67 (176)	1.69 (179)	1.72 (174)	1.69 (178)	1.70 (176)	1.69 (175)	1.69 (170)	1.68 (162)
Sub:*H*-Sub:O	2.74 (112)	2.64 (113)	2.47 (118)	2.40 (118)	2.47 (116)	4.57	4.48	4.42	4.36	4.47
Sub:**O**-Thr40:NH	3.96 (131)	3.93 (144)	3.20 (139)	3.20 (139)	3.22 (137)	4.05	3.86	3.77	3.94	4.24
Sub:**O**-Thr40:OH	3.58 (137)	3.57 (140)	2.92 (131)	2.81 (128)	2.75 (122)	4.00	3.77	3.64	3.61	3.77

[a] Distances are given in Å. Angles for the corresponding hydrogen bonds and the nucleophilic attack (Sub:**O**⋯SEA:C1=O) are given in degrees (in parentheses). See Figure 4 of the main text for conventions on the atom labels.

4.3. QM(B3LYP/TZVP)/CHARMM results for the transformation of *S*-propranolol in binding mode I

Table S14

QM(B3LYP/TZVP) and MM(CHARMM) energies in kcal/mol (relative to the MCC) for the transformation of *S*-propranolol in binding mode I via the TI-2 configuration OSI[a].

Stationary point	OSI			
	QM energy		MM energy	
MCC	0		0	
TS1	13.2	(13.2)	-1.6	(-1.6)
TI-2	-2.1		2.3	
TS2	1.2	(3.3)	1.1	(-1.2)
PDC	-4.0		1.2	

[a] Activation barriers relative to the preceding minima are given in parentheses

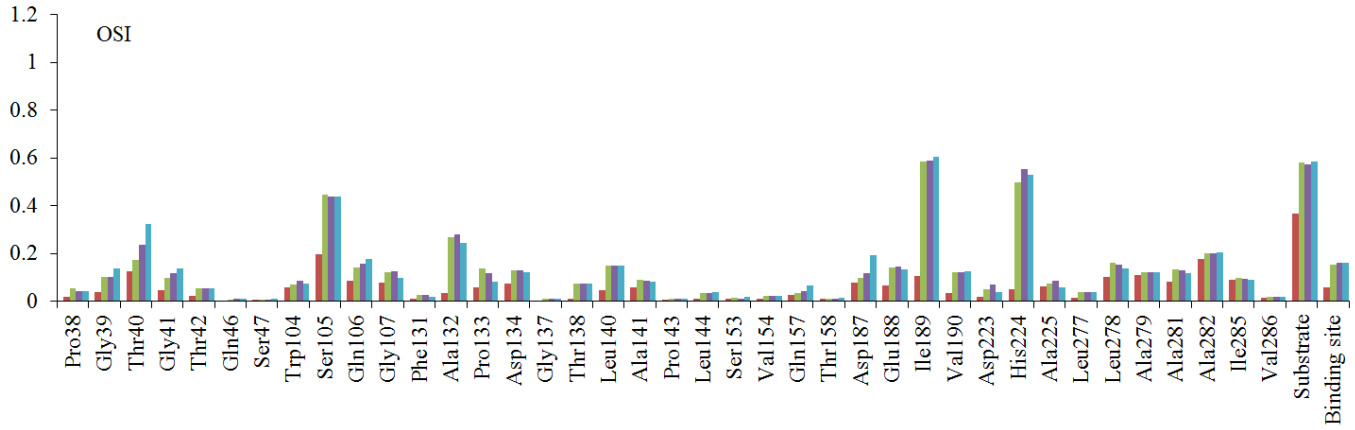

Figure S32. RMSD (in Å, with respect to the MCC) of the residues within 5 Å of the substrate at the stationary points along the reaction profile of OSI: TS1 (red), TI-2 (green), TS2 (violet) and PDC (blue). Only heavy atoms were considered. The RMSD for the substrate and the CalB binding site is also shown. The RMSD for the binding site was computed considering all residues within 5 Å of the substrate.

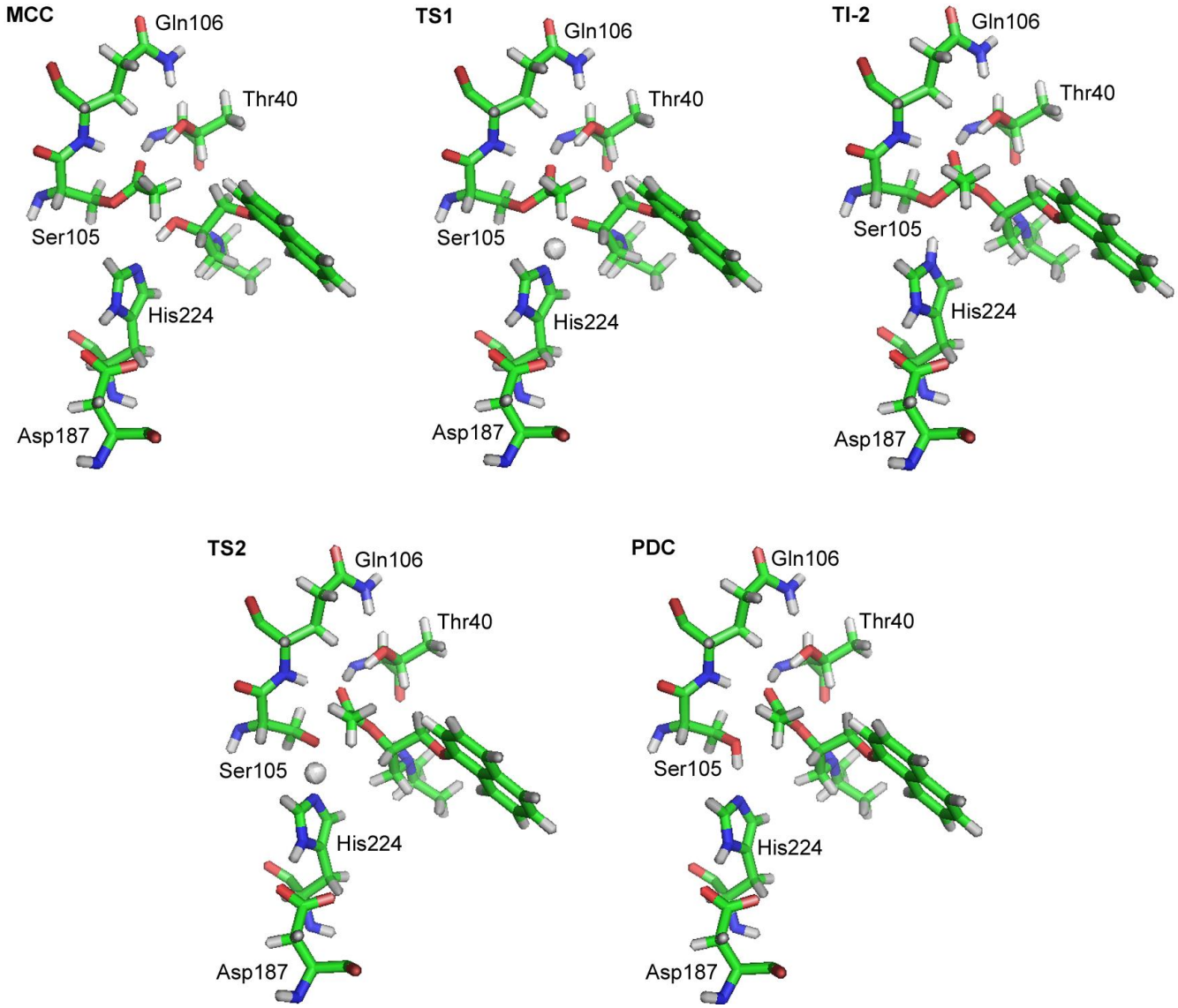

Figure S33. Stationary points along the energy profile for the conversion of *S*-propranolol to *S*-acetyl-propranolol via the TI-2 OSI. The formation of TI-2 is accompanied by the displacement of the alcohol oxygen toward the oxyanion hole.

Table S15

Distribution of dihedral angles characterizing TI-2[a] at the stationary points along the reaction profile obtained at the B3LYP(TZVP)/CHARMM level for the transformation of *S*-propranolol in binding mode I via TI-2 OSI.

Dihedral (°)	**OSI**				
	MCC	**TS1**	**TI-2**	**TS2**	**PDC**
ω_1	4	8	9	11	19
ω_2	113	102	153	162	170
ω_3	172	-178	141	143	144
ω_4	62	64	66	67	67
ω_5	-167	-170	177	174	171
ω_6	-65	-62	-79	-79	-79
ω_7	176	176	-180	179	177
ω_8	-88	-89	-116	-113	-108
ω_9	157	159	-172	-172	-173

[a] ω_1-ω_3 are the dihedral angles directly involved in the formation of TI-2. ω_4-ω_9 are the dihedral angles involving the propranolol molecule. See Figure S1.

Table S16

Relevant interatomic distances and bond angles corresponding to the stationary points along the reaction profile obtained at the B3LYP(TZVP)/CHARMM level for the transformation of *S*-propranolol in binding mode I via TI-2 OSI[a].

Distance (Å)	**OSI**				
	MCC	**TS1**	**TI-2**	**TS2**	**PDC**
Asp187:O_D-His224:H_{ND}	1.88 (166)	1.76 (166)	1.61 (172)	1.65 (173)	1.72 (174)
His224:**H**-SEA:Oγ	-	-	1.71 (168)	1.39 (171)	1.02
SEA:C1-SEA:Oγ	1.33	1.38	1.59	2.03	2.44
His224:Nε-His224:**H**	1.82 (173)	1.10 (169)	1.05	1.14 (171)	1.59 (172)
His224:**H**-Sub:**O**	1.00	1.57	3.16 (140)	-	-
SEA:C1-Sub:**O**	2.71 (95)	2.04 (106)	1.44 (109)	1.37 (114)	1.33 (116)
SEA:C1-SEA:O	1.23	1.24	1.29	1.25	1.23
SEA:O-Gln106:NH	1.96 (151)	1.94 (160)	1.71 (170)	1.79 (166)	1.94 (161)
SEA:O-Thr40:NH	2.00 (168)	1.93 (168)	1.74 (171)	1.77 (169)	1.83 (167)
SEA:O-Thr40:OH	1.72 (171)	1.71 (171)	1.68 (174)	1.71 (174)	1.72 (171)
Sub:*H*-Thr40:O	3.27 (126)	3.31 (117)	2.53 (141)	2.52 (142)	2.53 (141)
Sub:**O**-Thr40:NH	3.91 (128)	3.76 (137)	2.92 (131)	2.93 (131)	2.97 (130)
Sub:**O**-Thr40:OH	3.76 (130)	3.61 (140)	2.88 (129)	2.90 (127)	2.95 (124)

[a] Distances are given in Å. Angles for the corresponding hydrogen bonds and the nucleophilic attack (Sub:**O**···SEA:C1=O) are given in degrees (in parentheses). See Figure 4 of the main text for conventions on the atom labels.

4.4. QM(B3LYP/TZVP)/CHARMM results for the transformation of *S*-propranolol in binding mode II

Table S17

QM(B3LYP/TZVP) and MM(CHARMM) energies in kcal/mol (relative to the MCC) for the transformation of *S*-propranolol in binding mode II via the TI-2 configurations OSII-OSIV[a].

Stationary point	OSII				OSIII				OSIV			
	QM energy		MM energy		QM energy		MM energy		QM energy		MM energy	
MCC	0		0		0		0		0		0	
TS1	14.2	(14.2)	-3.1	(-3.1)	12.4	(12.4)	2.0	(2.0)	18.0	(18.0)	-2.3	(-2.3)
TI-2	7.9		-2.7		3.1		1.7		12.7		-0.6	
TS2	14.2	(6.3)	-1.8	(0.9)	7.2	(4.2)	1.2	(-0.5)	14.2	(1.5)	-0.6	(0.0)
PDC	9.2		0.7		-0.4		2.2		6.0		0.9	

[a] Activation barriers relative to the preceding minima are given in parentheses

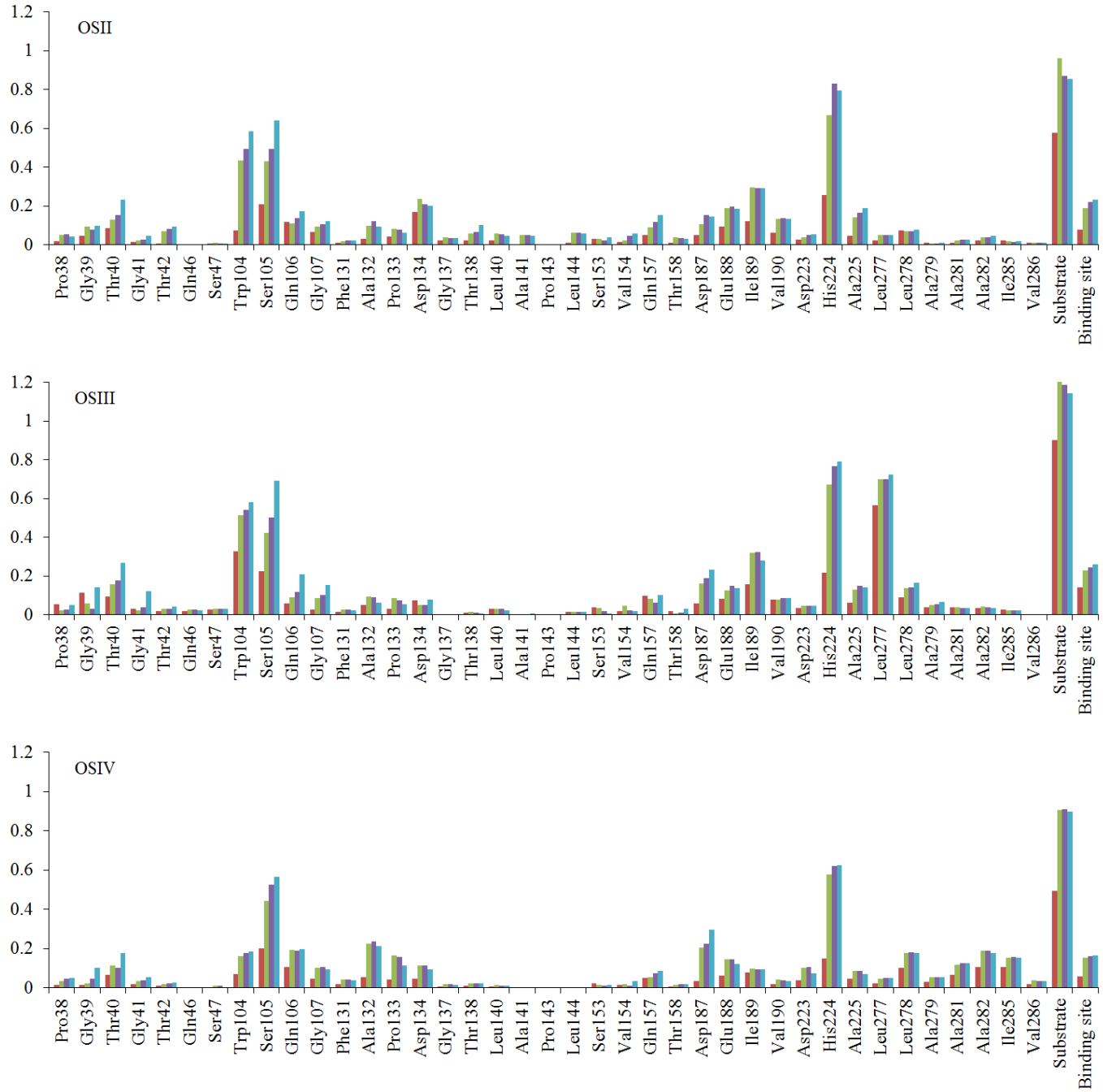

Figure S34. RMSD (in Å, with respect to the MCC) of the residues within 5 Å of the substrate at the stationary points along the reaction profiles of OSII-IV: TS1 (red), TI-2 (green), TS2 (violet) and PDC (blue). Only heavy atoms were considered. The RMSD for the substrate and the CalB binding site is also shown. The RMSD for the binding site was computed considering all residues within 5 Å of the substrate.

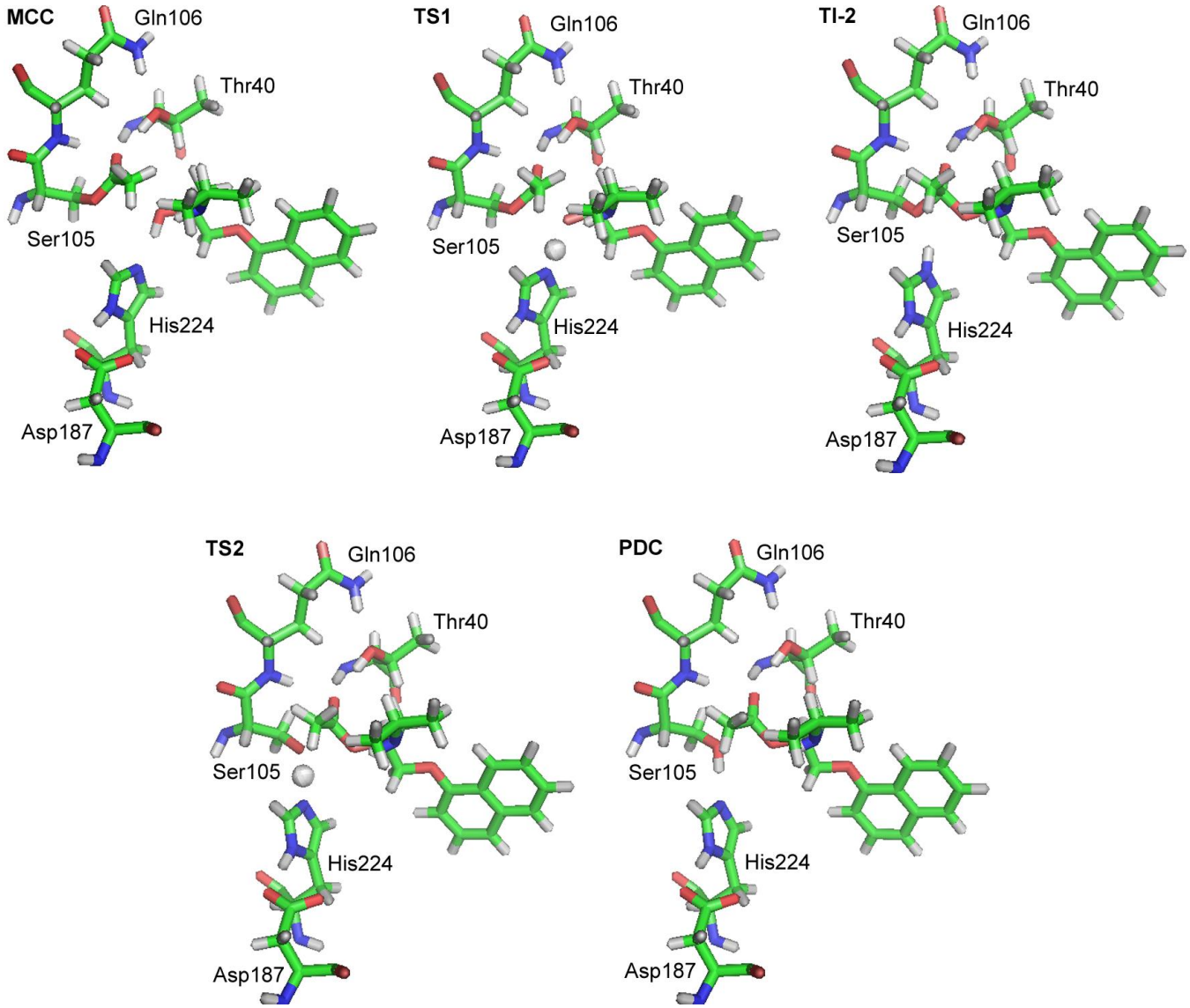

Figure S35. Stationary points along the energy profile for the conversion of *S*-propranolol to *S*-acetyl-propranolol via TI-2 OSII.

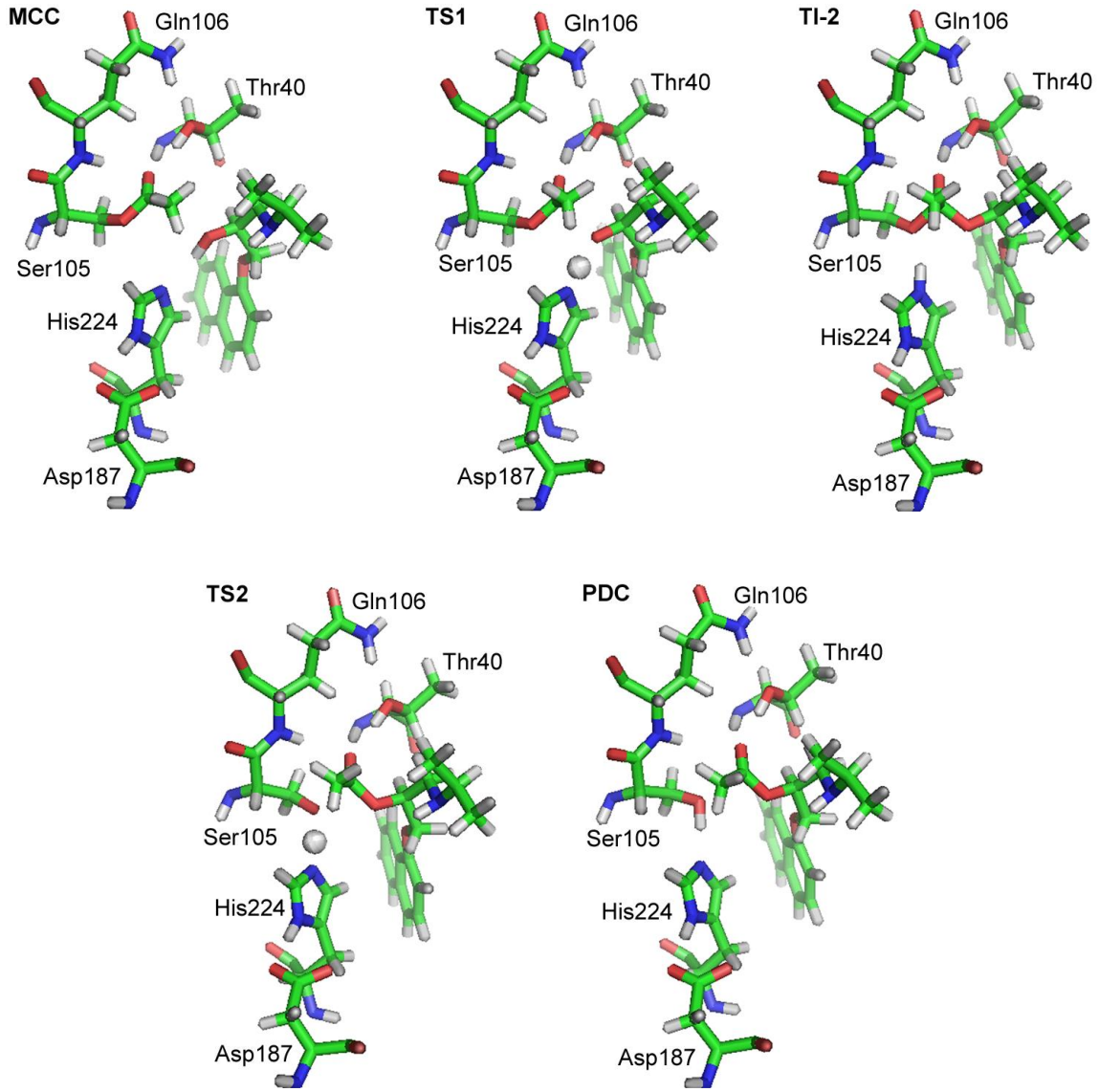

Figure S36. Stationary points along the energy profile for the conversion of *S*-propranolol to *S*-acetyl-propranolol via TI-2 OSIII.

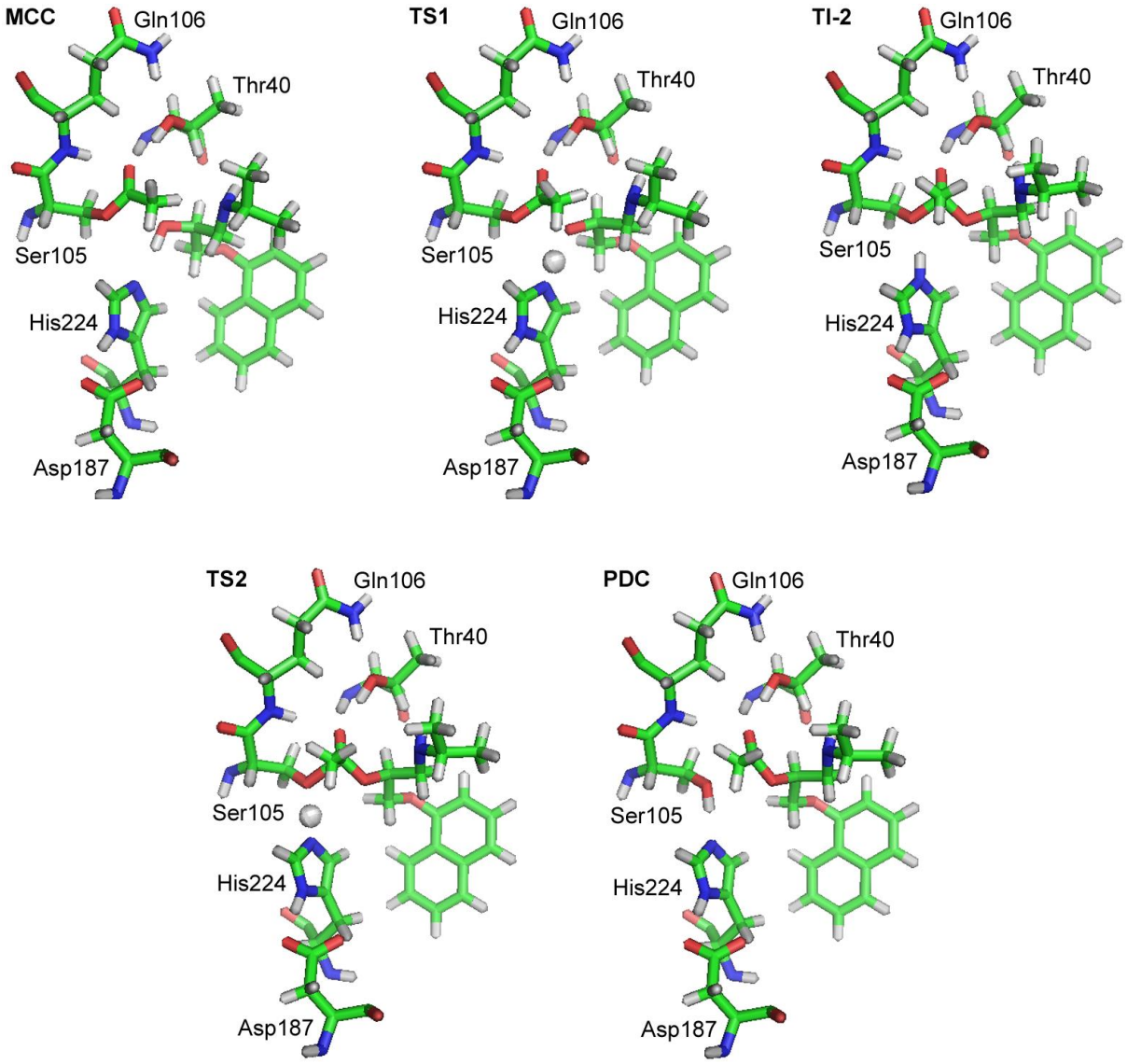

Figure S37. Stationary points along the energy profile for the conversion of *S*-propranolol to *S*-acetyl-propranolol via TI-2 OSIV.

Table S18

Distribution of dihedral angles characterizing TI-2[a] at the stationary points along the reaction profiles obtained at the B3LYP(TZVP)/CHARMM level for the transformation of *S*-propranolol in binding mode II via the TI-2 configurations OSII-OSIV.

Dihedral (°)	OSII					OSIII					OSIV				
	MCC	TS1	TI-2	TS2	PDC	MCC	TS1	TI-2	TS2	PDC	MCC	TS1	TI-2	TS2	PDC
ω_1	-3	-3	-21	-20	-34	2	-4	-17	-20	-36	12	21	4	-7	-1
ω_2	59	39	30	34	26	24	27	22	17	13	74	40	17	8	20
ω_3	43	66	73	73	76	72	71	80	85	85	54	89	105	113	106
ω_4	58	48	48	48	47	68	63	64	62	62	-77	-79	-60	-59	-59
ω_5	-169	-163	-158	-156	-153	-166	-172	-173	-166	-157	173	161	164	157	153
ω_6	-86	-87	-82	-83	-88	-163	-167	-166	-166	-165	-177	-177	-172	-170	-167
ω_7	-167	-163	-160	-158	-156	87	94	88	96	103	166	178	-180	-180	179
ω_8	-177	177	-178	-177	-176	-145	-152	-160	-166	-169	91	94	101	98	96
ω_9	-168	-159	-165	-165	-167	176	179	-175	-174	-177	62	60	63	67	70

[a] ω_1-ω_3 are the dihedral angles directly involved in the formation of TI-2. ω_4-ω_9 are the dihedral angles involving the propranolol molecule. See Figure S1.

Table S19

Relevant interatomic distances and bond angles corresponding to the stationary points along the reaction profiles obtained at the B3LYP(TZVP)/CHARMM level for the transformation of *S*-propranolol in binding mode II via the TI-2 configurations OSII-OSIV[a].

Distance (Å)	**OSII**					**OSIII**					**OSIV**				
	MCC	**TS1**	**TI-2**	**TS2**	**PDC**	**MCC**	**TS1**	**TI-2**	**TS2**	**PDC**	**MCC**	**TS1**	**TI-2**	**TS2**	**PDC**
Asp187:O_D-His224:H_{ND}	1.81 (170)	1.62 (171)	1.52 (175)	1.59 (176)	1.66 (175)	1.98 (168)	1.75 (170)	1.58 (176)	1.63 (177)	1.70 (176)	1.82 (168)	1.68 (167)	1.54 (174)	1.58 (175)	1.66 (176)
His224:**H**-SEA:Oγ	-	-	1.76 (151)	1.20 (167)	1.02	-	-	1.67 (164)	1.33 (172)	1.02	-	-	1.66 (164)	1.41 (171)	1.02
SEA:C1-SEA:Oγ	1.33	1.38	1.52	1.96	2.33	1.33	1.36	1.55	1.99	2.52	1.34	1.39	1.57	1.92	2.44
His224:Nε-His224:**H**	1.77 (168)	1.11 (171)	1.04	1.28 (167)	1.60 (168)	2.11 (147)	1.13 (170)	1.05	1.17 (172)	1.64 (176)	1.90 (173)	1.11 (176)	1.05	1.12 (171)	1.59 (173)
His224:**H**-Sub:**O**	1.00	1.48	2.34 (130)	-	-	0.98	1.45	2.62 (132)	-	-	0.99	1.49	2.46 (128)	-	-
SEA:C1-Sub:**O**	2.75 (100)	2.05 (109)	1.49 (118)	1.39 (122)	1.35 (124)	3.11 (101)	2.22 (107)	1.48 (118)	1.38 (122)	1.34 (124)	2.73 (94)	1.98 (108)	1.47 (118)	1.38 (122)	1.33 (124)
SEA:C1-SEA:O	1.22	1.24	1.28	1.24	1.22	1.23	1.24	1.29	1.24	1.22	1.23	1.25	1.29	1.25	1.23
SEA:O-Gln106:NH	1.92 (149)	2.01 (155)	2.02 (160)	2.15 (153)	2.33 (143)	2.07 (148)	2.10 (151)	2.06 (160)	2.20 (152)	2.59 (137)	1.86 (154)	1.95 (163)	2.02 (167)	2.14 (162)	2.47 (155)
SEA:O-Thr40:NH	1.80 (170)	1.78 (169)	1.80 (168)	1.88 (164)	2.12 (158)	1.95 (168)	1.98 (168)	1.87 (170)	1.99 (166)	2.33 (158)	1.90 (165)	1.80 (168)	1.77 (168)	1.83 (164)	1.95 (157)
SEA:O-Thr40:OH	1.72 (170)	1.74 (169)	1.74 (170)	1.76 (168)	1.72 (168)	1.73 (174)	1.74 (172)	1.72 (175)	1.72 (177)	1.66 (179)	1.70 (171)	1.71 (169)	1.72 (171)	1.73 (168)	1.71 (164)
Sub:*H*-Sub:O	3.89	3.89	3.82	3.75	3.72	4.33	4.51	4.43	4.38	4.30	4.19	4.32	4.71	4.70	4.69

[a] Distances are given in Å. Angles for the corresponding hydrogen bonds and the nucleophilic attack (Sub:**O**⋯SEA:C1=O) are given in degrees (in parentheses). See Figure 4 of the main text for conventions on the atom labels.

4.5. QM/MM results at different levels of theory

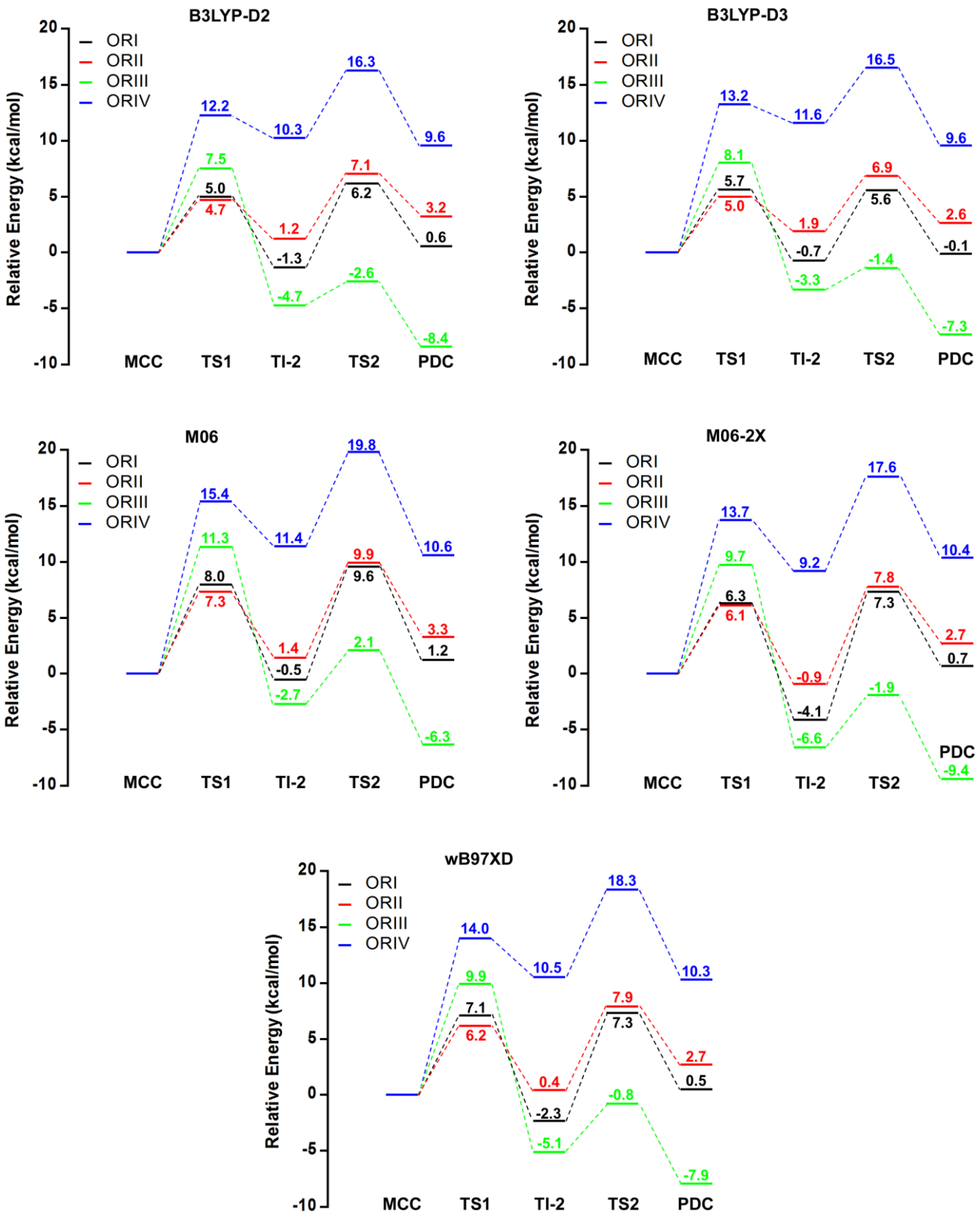

Figure S38. QM/MM energies for the stationary points along the reaction profiles of *R*-propranolol evaluated with different DFT methods in single-point calculations at the B3LYP(TZVP)/CHARMM optimized structures.

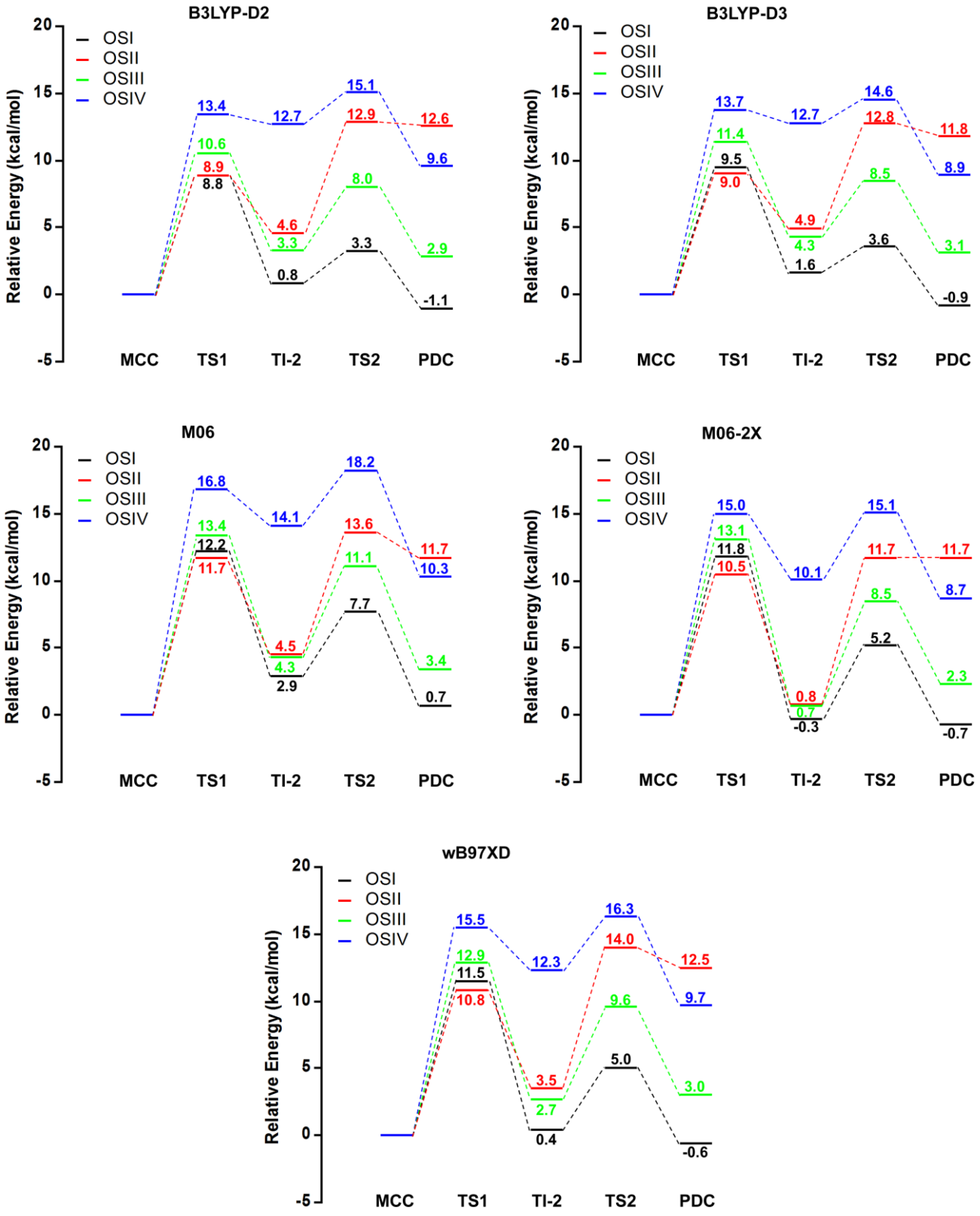

Figure S39. QM/MM energies for the stationary points along the reaction profiles of *S*-propranolol evaluated with different DFT methods in single-point calculations at the B3LYP(TZVP)/CHARMM optimized structures.

5. References

[1] Ryckaert, J.-P.; Ciccotti, G.; Berendsen, H. J. *J. Comput. Phys.* **1977,** 23, 327–341.

[2] Stote, R. H.; States, D. J.; Karplus, M. *J. Chim. Pys.* **1991,** 88, 2419-2433.

[3] Escorcia, A. M.; Molina, D.; Daza, M. C.; Doerr, M. *J. Mol. Catal. B: Enzym.* **2013,** 98, 21-29.

[4] Macias, A. T.; Mackerell, A. D. Jr. *J. Comput. Chem.* **2005,** 26, 1452-1463.

[5] Nishio, M. *Phys. Chem. Chem. Phys.* **2011,** 13, 13873–13900.

[6] Haeffner, F.; Norin, T.; Hult, K. *Biophys. J.* **1998,** 74, 1251-1262.

[7] Nyhlén, J.; Martín-Matute, B.; Sandström, A. G.; Bocola, M.; Bäckvall, J. *ChemBioChem* **2008,** 9, 1968–1974.

[8] Schulz, T.; Pleiss, J.; Schmid, R.D. *Protein Sci.* **2000,** 9, 1053–1062.

[9] Syrén, P-O.; Hult, K. *Chembiochem.* **2010,** 11, 802-810.